Structural MRI predicts clinical progression in presymptomatic genetic frontotemporal dementia: findings from the GENetic Frontotemporal dementia Initiative cohort

Martina Bocchetta PhD[1,2], Emily G. Todd MRes[1], Arabella Bouzigues MSc[1], David M. Cash PhD[1,3], Jennifer M. Nicholas PhD[4], Rhian S. Convery MSc[1], Lucy L. Russell PhD[1], David L. Thomas PhD[1,5], Ian B. Malone PhD[1], Juan Eugenio Iglesias PhD[3,6,7], John C. van Swieten MD PhD[8], Lize C. Jiskoot PhD[8], Harro Seelaar MD PhD[8], Barbara Borroni MD[9], Daniela Galimberti PhD[10,11], Raquel Sanchez-Valle PhD[12], Robert Laforce Jr MD PhD[13], Fermin Moreno MD PhD[14], Matthis Synofzik MD[15,16], Caroline Graff MD PhD[17,18], Mario Masellis MD PhD[19], Maria Carmela Tartaglia MD[20], James B. Rowe FRCP PhD[21], Rik Vandenberghe MD PhD[22], Elizabeth Finger MD[23], Fabrizio Tagliavini MD[24], Alexandre de Mendonça MD PhD[25], Isabel Santana MD PhD[26], Chris R. Butler FRCP PhD[27], Simon Ducharme MD[28], Alexander Gerhard MRCP MD[29,30], Adrian Danek MD[31], Johannes Levin MD[31], Markus Otto MD[32], Sandro Sorbi MD[33,34], Isabelle Le Ber MD PhD[35,36,37], Florence Pasquier MD PhD[38,39,40], Jonathan D. Rohrer FRCP PhD[1], Genetic Frontotemporal dementia Initiative (GENFI)

Affiliations:

[1]Dementia Research Centre, Department of Neurodegenerative Disease, UCL Queen Square Institute of Neurology, University College London, London, United Kingdom

[2]Centre for Cognitive and Clinical Neuroscience, Division of Psychology, Department of Life Sciences, College of Health, Medicine and Life Sciences, Brunel University London, London, United Kingdom

[3]Centre for Medical Image Computing, Department of Medical Physics and Biomedical Engineering, University College London, London, United Kingdom

[4]Department of Medical Statistics, London School of Hygiene and Tropical Medicine, London, United Kingdom

[5]Neuroradiological Academic Unit, Department of Brain Repair and Rehabilitation, UCL Queen Square Institute of Neurology, University College London, London, United Kingdom

[6]Martinos Center for Biomedical Imaging, Massachusetts General Hospital and Harvard Medical School, Charlestown, MA, USA

[7]Computer Science and Artificial Intelligence Laboratory, Massachusetts Institute of Technology, Cambridge, MA, USA

[8]Department of Neurology and Alzheimer center, Erasmus Medical Center Rotterdam, Rotterdam, the Netherlands

[9]Centre for Neurodegenerative Disorders, Neurology Unit, Department of Clinical and Experimental Sciences, University of Brescia, Brescia, Italy

[10]Department of Biomedical, Surgical and Dental Sciences, University of Milan, Milan, Italy

[11]Fondazione IRCCS Ca' Granda, Ospedale Maggiore Policlinico, Milan, Italy

[12]Neurology Department, Hospital Clinic, Institut d'Investigacions Biomèdiques, Barcelona, Spain

[13]Clinique Interdisciplinaire de Mémoire, Département des Sciences Neurologiques, CHU de Québec, Faculté de Médecine, Université Laval, Québec, Canada

[14]Hospital Universitario Donostia, San Sebastian, Spain

[15]Division Translational Genomics of Neurodegenerative Diseases, Hertie Institute for Clinical Brain Research (HIH), University of Tübingen, Tübingen, Germany

[16]German Center for Neurodegenerative Diseases (DZNE), Tübingen, Germany

[17]Karolinska Institutet, Department NVS, Division of Neurogeriatrics, Stockholm, Sweden

[18]Unit for Hereditary Dementia, Theme Aging, Karolinska University Hospital-Solna Stockholm, Stockholm, Sweden

[19]Campbell Cognitive Neurology Research Unit, Sunnybrook Research Institute, Toronto, ON, Canada

[20]Toronto Western Hospital, Tanz Centre for Research in Neurodegenerative Disease, Toronto, ON, Canada

[21]Department of Clinical Neurosciences and Cambridge University Hospitals NHS Trust and Medical Research Council Cognition and brain Sciences Unit, University of Cambridge, Cambridge, United Kingdom

[22]Laboratory for Cognitive Neurology, Department of Neurosciences, KU Leuven, Leuven, Belgium

[23]Department of Clinical Neurological Sciences, University of Western Ontario, London, ON, Canada

[24]Fondazione Istituto di Ricovero e Cura a Carattere Scientifico, Istituto Neurologico Carlo Besta, Milan, Italy

[25]Faculty of Medicine, University of Lisbon, Lisbon, Portugal

[26]Neurology Department, Centro Hospitalar e Universitário de Coimbra, Coimbra, Portugal

[27]Department of Clinical Neurology, University of Oxford, Oxford, United Kingdom

[28]Department of Neurology and Neurosurgery, McGill University, Montreal, Quebec, Canada

[29]Division of Neuroscience and Experimental Psychology, Wolfson Molecular Imaging Centre, University of Manchester, Manchester, United Kingdom

[30]Departments of Geriatric Medicine and Nuclear Medicine, University of Duisburg-Essen, Essen, Germany

[31]Neurologische Klinik und Poliklinik, Ludwig-Maximilians-Universität, Munich; German Center for Neurodegenerative Diseases (DZNE), Munich; Munich Cluster of Systems Neurology, Munich, Germany

[32]Department of Neurology, University Hospital Ulm, Ulm, Germany

[33]Department of Neuroscience, Psychology, Drug Research and Child Health, University of Florence, Florence, Italy

[34]IRCCS Fondazione Don Carlo Gnocchi, Florence, Italy

[35]Sorbonne Université, Paris Brain Institute – Institut du Cerveau– ICM, Inserm U1127, CNRS UMR 7225, AP-HP - Hôpital Pitié-Salpêtrière, Paris, France

[36]Centre deréférence des démences rares ou précoces, IM2A, Département de Neurologie, AP-HP - Hôpital Pitié-Salpêtrière, Paris, France

[37]Département de Neurologie, AP-HP - Hôpital Pitié-Salpêtrière, Paris, France

[38]Univ Lille, Lille, France

[39]Inserm 1172, Lille, France

[40]CHU, CNR-MAJ, Labex Distalz, LiCENDLille, Lille, France

*See Appendix for a list of GENFI consortium members.

Corresponding author

Dr Martina Bocchetta, Dementia Research Centre, Department of Neurodegenerative Disease, UCL Queen Square Institute of Neurology, 8-11 Queen Square, London, WC1N 3BG, United Kingdom; m.bocchetta@ucl.ac.uk

Running title: MRI predicts progression in genetic FTD

Abstract

Biomarkers that can predict disease progression in individuals with genetic frontotemporal dementia are urgently needed. We aimed to identify whether baseline MRI-based grey and white matter abnormalities are associated with different clinical progression profiles in presymptomatic mutation carriers in the GENetic Frontotemporal dementia Initiative.

387 mutation carriers were included (160 *GRN*, 160 *C9orf72*, 67 *MAPT*), together with 240 non-carrier cognitively normal controls. Cortical and subcortical grey matter volumes were generated using automated parcellation methods on volumetric 3T T1-weighted MRI scans, while white matter characteristics were estimated using diffusion tensor imaging. Mutation carriers were divided into two disease stages based on their global CDR®+NACC-FTLD score: presymptomatic (0 or 0.5) and fully symptomatic (1 or greater). W-scores in each grey matter volumes and white matter diffusion measures were computed to quantify the degree of abnormality compared to controls for each presymptomatic carrier, adjusting for their age, sex, total intracranial volume, and scanner type. Presymptomatic carriers were classified as "normal" or "abnormal" based on whether their grey matter volume and white matter diffusion measure w-scores were above or below the cut point corresponding to the 10^{th} percentile of the controls. We then compared the change in disease severity between baseline and one year later in both the "normal" and "abnormal" groups within each genetic subtype, as measured by the CDR®+NACC-FTLD sum-of-boxes score and revised Cambridge Behavioural Inventory total score.

Overall, presymptomatic carriers with normal regional w-scores at baseline did not progress clinically as much as those with abnormal regional w-scores. Having abnormal grey or white matter measures at baseline was associated with a statistically significant increase in the CDR®+NACC-FTLD of up to 4 points in *C9orf72* expansion carriers, and 5 points in the *GRN* group as well as a statistically significant increase in the revised Cambridge Behavioural Inventory of up to 11 points in *MAPT*, 10 points in *GRN,* and 8 points in *C9orf72* mutation carriers.

Baseline regional brain abnormalities on MRI in presymptomatic mutation carriers are associated with different profiles of clinical progression over time. These results may be helpful to inform stratification of participants in future trials.

Keywords: genetic frontotemporal dementia, MRI imaging, brain volumetry, diffusion imaging, presymptomatic stage

List of abbreviations:

aCR: anterior corona radiata

aIC: anterior part of the internal capsule

ALS: amyotrophic lateral sclerosis

bCC: body of the corpus callosum

bvFTD: behavioural variant of frontotemporal dementia

CBI-R: revised version of the Cambridge Behavioural Inventory

CBS: corticobasal syndrome

C9orf72: chromosome 9 open reading frame 72

DLPFC: dorsolateral prefrontal cortex

EC: external capsule

FA fractional anisotropy

FTD: frontotemporal dementia

gCC: genu of the corpus callosum

GENFI: GENetic Frontotemporal dementia Initiative

GIF: geodesic information flow

GM: grey matter

GRN: progranulin

JHU: John Hopkins University

i-tub: inferior tuberal

LD: laterodorsal

LGN: lateral geniculate nucleus

MAPT: microtubule-associated protein tau

MD: mean diffusivity

MED PARIETAL: medial parietal

MGN: medial geniculate nucleus

N/A: not applicable

N/I: not included in the analyses

NOS: not otherwise specified

pCR: posterior corona radiata

pIC: posterior part of the internal capsule

PPA: primary progressive aphasia

PSP: progressive supranuclear palsy

pTR: posterior thalamic radiation

rIC: retrolenticular part of the internal capsule

ROI: region of interest

sCC: splenium of the corpus callosum

sCR: superior corona radiata

SD: standard deviation

SLF: superior longitudinal fasciculus

SS: sagittal stratum

s-tub: superior tuberal

TIV: total intracranial volume

UF: uncinate fasciculus

VMPFC: ventromedial prefrontal cortex

WM: white matter

Introduction

Genetic frontotemporal dementia (FTD) is a progressive and heterogeneous neurodegenerative disease most frequently caused by an autosomal dominant genetic mutation in the microtubule-associated protein tau (*MAPT*), progranulin (*GRN*), or chromosome 9 open reading frame 72 (*C9orf72*).[1] Changes in grey and white matter regions measured by magnetic resonance imaging (MRI) have been reported many years before symptoms develop in previous studies,[2-4] but the exact relationship of such brain changes to clinical progression is yet to be fully understood. This is particularly relevant in current research, considering the need for robust biomarkers to allow accurate measurement of disease onset and progression in the context of clinical trials.

Using data from the GENetic FTD Initiative (GENFI) cohort, we aimed to localise and quantify the specific pattern of subregional grey and white matter abnormalities in the prodromal and symptomatic stages of genetic FTD, and how these abnormalities relate to progression of symptoms in presymptomatic mutation carriers.

Materials and methods

At the time of the fifth data freeze in the GENFI study, 850 participants had been recruited as part of the second phase (03/03/2015-31/05/2019) across 24 centres in the United Kingdom, Canada, Italy, the Netherlands, Sweden, Portugal, Germany, France, Spain, and Belgium, of whom 710 had volumetric T1-weighted and diffusion weighted MRI acquired on a 3T scanner. 83 of these participants were excluded as their scans were of unsuitable quality due to motion, incomplete spatial coverage or other imaging artefacts, for pathology unlikely to be attributed to FTD, or if they were carriers of mutations in one of the rarer genetic causes of FTD. All the remaining 627 participants were known to be either a carrier of a pathogenic expansion in *C9orf72* or of a pathogenic mutation in *GRN* or *MAPT* (n=387), or were non-carrier first-degree relatives (n=240), who therefore acted as controls within the study. Participants have been screened and genotyped at their local sites for the most common pathogenic genetic mutations for FTD. All aspects of the study were approved by the local ethics committee for each of the GENFI sites, and written informed consent was obtained from all participants.

All participants underwent a standardized clinical assessment as described previously.[2] This included the CDR® plus NACC FTLD,[5] a measure of disease severity, from which both a global score and a sum of boxes score can be calculated. The global score can be used to stage mutation carriers, with those with a score of 0 or 0.5 considered as “presymptomatic”, and

those with a score of 1, 2 or 3 considered as "fully symptomatic" (**Table 1**). Additionally, the revised version of the Cambridge Behavioural Inventory (CBI-R)[6] was also completed as a measure of behavioural impairment.

Participants underwent MRI scans on five types of 3T system from different vendors (Siemens Trio, Siemens Skyra, Siemens Prisma, Philips Achieva, GE Discovery MR750). Specific acquisition parameters are reported in the **Supplementary Table 1**.

T1-weighted processing

The processing was performed as previously described.[7] In brief, volumetric MRI scans were first bias field corrected and whole brain parcellated using the geodesic information flow (GIF) algorithm,[8] which is based on atlas propagation and label fusion. We combined regions of interest (ROIs) to calculate grey matter (GM) volumes of 13 ROIs of the cortex (**Figure 1**): orbitofrontal, dorsolateral (DLPFC) and ventromedial prefrontal (VMPFC), motor, insula, temporal pole, dorsolateral and medial temporal, cingulate, sensory, medial and lateral parietal, and occipital cortex. We used GIF and customised versions of specific Freesurfer modules[9-12] which accept the GIF parcellation as inputs[13-16] to calculate individual volumes for the following subcortical ROIs (**Figure 1**): i) basal ganglia (nucleus accumbens, caudate, putamen, and globus pallidus, ii) basal forebrain, iii) amygdala (5 regions: lateral nucleus, basal and paralaminar nucleus, accessory basal nucleus, cortico-amygdaloid transition area and the superficial nuclei), iv) hippocampus (7 regions: cornu ammonis CA1, CA2/CA3, CA4, dentate gyrus, subiculum, presubiculum, tail), v) thalamus (14 regions: anteroventral, laterodorsal (LD), lateral posterior, ventral anterior, ventral lateral anterior, ventral lateral posterior, ventral posterolateral, ventromedial, intralaminar, midline, mediodorsal, lateral geniculate (LGN), medial geniculate (MGN) and pulvinar). We computed the volumes for the hypothalamus (5 regions: anterior superior, anterior inferior, superior tuberal (s-tub), inferior tuberal (i-tub), posterior) using the deep convolutional neural network method described in Billot *et al*.[17] We also parcellated the cerebellum (separated into 12 regions: lobules I-IV, V, VI, VIIa-Crus I, VIIa-Crus II, VIIb, VIIIa, VIIIb, IX, X, vermis, and deep nuclei)[18-19], and brainstem (superior cerebellar peduncle, medulla, pons, and midbrain)[10]. We calculated the whole brain volume by summing the WM and GM regions extracted from GIF. We summed left and right volumes, and we computed the total intracranial volume (TIV) with SPM12 v6470 (Statistical Parametric Mapping, Wellcome Trust Centre for Neuroimaging, London, UK) running under Matlab R2014b (Math Works, Natick, MA, USA).[20] All segmentations were visually checked for quality with only one subject excluded from the cerebellar analyses due to the presence of an arachnoid cyst.

DTI acquisition and processing

The preprocessing was carried out with a combination of source tools described below, wrapped up by NiftyPipe (http://cmictig.cs.ucl.ac.uk/wiki/index.php/NiftyPipe) software packages. First, the multiple DWI acquisitions were merged with the FMRIB Software Library (FSL, v5.0.4).[21] Then, the images were corrected for eddy-current distortion and motion by performing an affine co-registration between the diffusion weighted images and the averaged b0 images, using FSL eddy function. [22] Susceptibility-induced image distortions were subsequently corrected using a unified field map and image registration-based approach.[23] We used the subject-specific structural T1-weighted image as the reference space, and the TIV binary mask extracted from GIF to restrict the analyses to the brain, and to improve the registration. Niftyfit[24] was used for the diffusion tensor fitting, which was estimated using the weighted least square method. Before the groupwise registration, the tensors were visually checked and prepared according to the approach reported in [http://dti-tk.sourceforge.net/pmwiki/pmwiki.php?n=Documentation.BeforeReg]. DTI-TK (http://dti-tk.sourceforge.net)[25-28] was used to spatially normalise the diffusion tensor volumes to a population-specific tensor template,[27,29] where the "IXI aging template"[31-33] was used for the template initialization, from an initial rigid registration, followed by non-linear registration (http://dti-tk.sourceforge.net/pmwiki/pmwiki.php?n=Documentation.Registration).[27,33]

We created maps of fractional anisotropy (FA) and mean diffusivity (MD) for each diffusion tensor image in the groupwise space. Using NiftyReg[34] we registered the FA image from the study-specific template with the John Hopkins University (JHU)[35] FA image provided in FSL, applying an affine transformation first, followed by a non-linear registration using a B-spline. The mean FA and MD were then extracted for the following WM tracts from the JHU atlas[35] using DTI-TK (**Figure 1**): uncinate fasciculus (UF), superior longitudinal fasciculus (SLF), cingulum, sagittal stratum (SS), posterior thalamic radiation (pTR), anterior (aCR), posterior (pCR) and superior (sCR) corona radiata, external capsule (EC), anterior (aIC), posterior (pIC) and retrolenticular part (rIC) of the internal capsule, and genu (gCC), body (bCC) and splenium of the corpus callosum (sCC). Left and right values were averaged to obtain one bilateral value per metric (FA and MD) per tract.

Statistical analyses

We computed w-scores for each of the volumes and diffusion indexes for the GM and WM ROIs. The w-score is a metric that quantifies the extent of abnormalities in each index for each mutation carrier after adjusting for the effects of age, sex,

TIV, and scanner type. To calculate the w-score, first linear regression models were carried out in controls to relate the value of each index to age, sex, TIV, and scanner type. After fitting the model, predicted values of the index were produced for the mutation carriers using the control model equation, given the mutation carriers age, sex, TIV, and the scanner type. Finally, the w-scores were calculated using the following formula:

$$wscore_i = \frac{x_i - \hat{x_i}}{\sigma}$$

Where,

$wscore_i$ is the w-score for the ith mutation carrier

x_i is the observed value of the index for the ith mutation carrier

$\hat{x}_i$ is the predicted value of the index for the ith mutation carrier based on the control linear regression model, given the mutation carriers age, sex, TIV and the scanner type

σ is the square root of the residual variance from the linear regression model in controls

The w-scores have a similar interpretation to Z-scores: in the control group they have a mean value of 0 and a standard deviation of 1; a w-score of −1.960 corresponds to the 2.5th percentile of the controls, −1.645 to the 5th percentile, -1.282 to the 10th percentile, and -0.675 to the 25th percentile.

Statistical analyses were performed in Stata v.14 (Stata Statistical Software: College Station, TX: StataCorp LP) and SPSS v.26 software (SPSS Inc., Chicago, IL, USA). First, we calculated non-parametric percentile 95% confidence intervals using bootstrapping with 1000 replicates (as not all variables were normally distributed) to verify whether the GM and WM w-scores in the presymptomatic and symptomatic (as defined by CDR® plus NACC FTLD) subgroups within each genetic groups (*C9orf72*, *MAPT*, *GRN*) were each significantly different from 0, indicating the mean in the genetic group was below the mean of controls (or above 0 in the case of MD).

Then we focused on the presymptomatic carriers (excluding those scoring CDR® plus NACC FTLD≥1) and for each of the cortical, whole subcortical and WM ROIs we separated those with a w-score below and above −1.282 (or for MD above and below 1.282) ("abnormal" vs "normal", with "abnormal" corresponding to the 10th percentile of the controls), and we compared their CDR® plus NACC FTLD sum of boxes scores and their CBI-R total scores after one year. To investigate whether there was a difference in the clinical and behavioural scores over time in the "abnormal" vs "normal" groups for

each of the GM and WM ROIs, we performed a Wilcoxon Signed Rank exact test to compare baseline to follow-up scores for the presymptomatic carriers who had follow-up visits available at 12 months (*C9orf72* n=56; *MAPT* n=32; *GRN* n=69). We excluded groups with <3 carriers and we considered with caution non-significant results on groups with <6 carriers, as it is not possible for these comparisons to reach statistical significance on the Wilcoxon Signed Rank test.

Data availability

Data will be shared according to the GENFI data sharing agreement, after review by the GENFI data access committee with final approval granted by the GENFI steering committee.

Results

Baseline GM volumes

The results on the analyses for the w-scores on GM volumes at baseline are described in detail in the **Supplementary Material** and in **Supplementary Table 2**.

Briefly*, C9orf72* expansion carriers showed the most widespread GM differences (**Figure 2**), even at a presymptomatic stage. In particular, the thalamus was the structure with the most abnormal regions in presymptomatically, with the pulvinar showing w-scores below the 10th percentile of the controls.

Presymptomatic *MAPT* mutation carriers showed localised abnormal w-scores in the dorsolateral temporal cortex and in regions of the amygdala, hippocampus and thalamus (**Figure 3**). At the fully symptomatic stage, values were extremely low (<2.5th percentile) in all the temporal cortex, amygdala, hippocampus and insula, and in some regions of the hypothalamus (**Figure 3**).

Presymptomatic *GRN* mutation carriers showed significantly lower values in the temporal pole, presubiculum, and in the anterior superior cerebellum (**Figure 4**). Fully symptomatic carriers showed widespread cortical and subcortical involvement, with extremely low w-scores (<2.5th percentile) in the DLPFC, insula and motor cortex, and in the presubiculum, mediodorsal thalamus and posterior hypothalamus (**Figure 4**).

Baseline diffusion WM indices

Presymptomatic *C9orf72* expansion carriers showed both FA and MD values significantly different than controls in the SS, corpus callosum (genu and body), pTR, aCR, and EC (**Figure 5**). Symptomatic *C9orf72* expansion carriers showed

extremely abnormal values (<2.5th percentile) in the gCC and aCR for FA, and in the SS, corpus callosum (genu and body), aCR, sCR, cingulum, pTR, and aIC for MD (**Figure 5**).

Presymptomatic *MAPT* mutation carriers only showed significantly lower FA than controls in the aIC (**Figure 6**). Once symptoms were present, *MAPT* mutation carriers showed extremely abnormal values (<2.5th percentile) for the UF (both FA and MD), and SS (MD only) (**Figure 6**).

At a presymptomatic stage, *GRN* mutation carriers showed significantly lower FA than controls in the sCR, and significantly higher MD than controls in the UF and aCR (**Figure 7**). Fully symptomatic *GRN* mutation carriers showed abnormal FA and MD values in all tracts, with extremely abnormal values (<2.5th percentile) in the corpus callosum (genu and body), cingulum, aIC, and aCR for FA, and in nearly all tracts for MD (**Figure 7**).

Detailed description of the results is reported in the **Supplementary Material** and in **Supplementary Table 3**.

Progression

Figure 8 shows the longitudinal changes in the CDR®+NACC FTLD sum of boxes and CBI-R total scores over one year in the presymptomatic mutation carriers with w-scores of the *whole brain volume* above ("normal") and below ("abnormal") the 10th percentile of the controls. For the CDR®+NACC FTLD sum of boxes, *C9orf72* and *GRN* mutation carriers showed significant increases within the "abnormal brain" subgroups (1 and 3 points respectively), with *GRN* mutation carriers also showing significant increases of 0.3 points in the subgroup with "normal" brain at baseline. The increase in 2 points for *MAPT* mutation carriers did not reach statistical significance, as there were only 4 carriers in the "abnormal brain" subgroup. Although both the *MAPT* and *GRN* "abnormal brain" subgroups showed a substantial increase in CBI-R of 16 and 11 points respectively, this was not statistically significant due to the small sample sizes for analysis of this measure (n=3 and 4). Overall, the magnitude of clinical changes in *C9orf72* expansion carriers was smaller than what seen in *MAPT* and *GRN* mutation carriers.

Supplementary Table 4 and **5** show the results of the longitudinal change in both the CDR® plus NACC FTLD sum of boxes and CBI-R total scores across the three genetic groups for all the individual GM and WM ROIs. Below we discuss the ROIs which showed the largest significant change in scores (i.e. most clinical progression) over time within the three genetic groups.

C9orf72 expansion carriers

The ROIs in which w-score abnormalities at baseline resulted in the highest significant increase in the CDR® plus NACC FTLD sum of boxes score were the DLFPC and motor cortex among the GM ROIs (+3 points, p-value≤0.016, **Supplementary Table 4 and 5**), and the MD in the UF (+4, p-value=0.031), gCC and aCR (+3, p-value≤0.031), together with the FA in the UF (+3, p-value=0.031) among the WM diffusion indexes (**Supplementary Table 4 and 5, Figure 9**). Except for a few regions (**Supplementary Table 4** and **5**), the subgroups with "normal" GM and WM ROIs at baseline showed a statistically significant increase no greater than 1 point.

The w-scores which led to the largest change over time in the CBI-R total score were the MD in the SS and the FA in the cingulum (6-8 points, p-value≤0.047), with similar values for the MD in the EC and gCC, although not reaching statistical significance as only 5 presymptomatic carriers were available for this analysis (**Figure 9** and **Supplementary Table 4 and 5**). For none of the GM ROIs, w-score abnormalities at baseline resulted in a statistically significant increase. However, the medial parietal, cingulate and nucleus accumbens led to a large change over time (7-10 points), which did not reach statistical significance given the small sample of carriers (n=3 and 5).

Carriers with normal regional w-scores at baseline did not progress on the CBI-R total scores after 12 months.

MAPT mutation carriers

No statistically significant increase was found for the CDR® plus NACC FTLD total score, which may be largely due to the small numbers in the abnormal subgroups. However, when looking at which abnormal w-scores resulted in the highest increase of 2 points, these were the motor, putamen and VMPFC, and the following among the WM diffusion indexes: gCC (both FA and MD), rIC, sCR, pCR, pTR, EC, SS, SLF (FA), and bCC and aCR (MD) (**Figure 9** and **Supplementary Table 4 and 5**).

Abnormal w-scores values in the occipital cortex and in the FA in the UF led to a significant increase of respectively 8 and 11 points in the CBI-R total scores over a year (p-value≤0.035, **Figure 9** and **Supplementary Table 4 and 5**). Other large increases, despite not reaching statistically significance, were seen in the abnormal values for the hypothalamus (+19), VMPFC (+17), putamen and motor cortex (+16), and for the FA in the gCC, pTR, SS (+15) and SLF (+13) (**Figure 9** and **Supplementary Table 4 and 5**).

Carriers with normal regional w-scores at baseline did not progress on the CDR® plus NACC FTLD or CBI-R total scores after 12 months.

GRN mutation carriers

The abnormal ROIs which showed the largest statistically significant increase in CDR® plus NACC FTLD sum of boxes scores were the MD in the gCC and EC (+4-5, p-value≤0.031), followed by MD in the aCR, FA in the aIC and aCR, and VMPFC, motor, lateral parietal, cingulate and hypothalamus (+3, p-value≤0.031) (**Figure 9** and **Supplementary Table 4 and 5**). Moreover, the small sample of carriers with abnormal w-scores in the DLPFC and globus pallidus led to a large change over time (+5-6 points).

The subgroups with "normal" GM and WM ROIs at baseline (except for MD in the sCC and aCR) showed statistically significant increase no greater than 1 point (**Figure 9** and **Supplementary Table 4 and 5**).

For the CBI-R total scores, a statistically significant increase of 10 points was seen if the baseline w-scores for the caudate or the FA in aCR were abnormal (p-value≤0.046), while a statistically significant increase of 8 and 9 points if the SLF (MD) and hypothalamus w-scores were abnormal (p-value≤0.016) (**Figure 9** and **Supplementary Table 4 and 5**). The small sample of carriers with abnormal w-scores at baseline also led to a large change over time, specifically in the globus pallidus (+18 points), hippocampus and gCC (MD) (+12), and DLPFC (+11).

The subgroups with "normal" ROIs at baseline in the following regions were showing a statistically significant increase of 1 or 2 points: VMPFC, dorsolateral temporal, temporal pole, medial parietal, insula, cerebellum, basal forebrain; bCC, sCC, pCR, cingulum (FA); and aIC, pIC, pTR, SS (MD).

Discussion

Using *in vivo* volumetric and diffusion MR imaging, we have quantified and localised the pattern of brain anomalies in a large cohort of presymptomatic and symptomatic carriers of *C9orf72*, *MAPT* and *GRN* mutations. Moreover, we were able to define which neuroimaging markers were associated with the largest clinical and behavioural changes over one year in presymptomatic mutation carriers.

C9orf72 expansion carriers showed the earliest and most widespread abnormalities in the brain, with the pulvinar and its posterior WM tracts being the most affected regions at the presymptomatic stage. These findings confirm what has been reported by previous studies, and in line with the role that the pulvinar plays in the development of psychotic symptoms in *C9orf72*.[3, 7, 36-42] The presence of such early and widespread changes in *C9orf72* could be linked to an abnormal development in the brain networks, or to a very early neurodegenerative process, as suggested by Lee *et al*.[36]

MAPT mutation carriers were confirmed to have early and very localised abnormality in the mediotemporal lobe, especially in the medial amygdala, and in regions linked to the limbic network.[7,43] The WM tracts mainly affected in *MAPT* mutation carriers are the UF, cingulum, SS and gCC, connecting the anterior and medial temporal lobe to the prefrontal and orbitofrontal cortex.[44] These tracts have been previously reported to be abnormal in cohorts of symptomatic mutation carriers,[3,45] but not presymptomatically.[41] The data of GM and WM differences in *MAPT* mutation carriers seems to suggest that abnormalities might come first in the anterior-medial temporal regions, with further spread not long before symptom onset via structural connectivity to the rest of the frontal and limbic areas, but multimodal longitudinal studies on large cohorts are needed to investigate this further.

GRN mutation carriers showed minor abnormalities at the presymptomatic stages, both in the GM (presubiculum, cerebellum and temporal pole) and WM (sCR, aCR and UF), in line with existing literature.[3,7,46] However, at the symptomatic stage the abnormalities were severe and widespread to cortical and subcortical regions, with all WM tracts severely abnormal.[2,3,47,48]

Overall, abnormalities in GM and WM regions seem to suggest that the brain is affected extremely early in *C9orf72* expansion carriers, presents early localised abnormalities in *MAPT* mutation carriers, and only shows changes at a later stage in *GRN* mutation carriers. The presence of abnormalities in *MAPT* and *GRN* mutation carriers closer to symptom onset is also reported by a longitudinal multimodal study.[49] The relationship between WM and GM changes detectable *in vivo* on MRI and the underlining pathological changes in the three genetic groups is still to be fully understood, especially considering the heterogeneity within the same genetic group. According to the "molecular nexopathy" paradigm,[50] within affected brain networks there could be preferentially vulnerable hubs that different abnormal proteins (tau in *MAPT*, TDP-

43 in *GRN* and *C9orf72*, with additional dipeptide repeat proteins in the latter) can differentially target and damage, leading to diverse symptoms and disease progression.

Across all the three genetic groups, presymptomatic carriers with normal w-scores for brain regions at baseline did not show large progression in their average clinical, cognitive, or behavioural scores after 12 months. Even when there was a significant change over time (such as in *GRN* and *C9orf72*), this was less than one point at the CDR® plus NACC FTLD total score, and less than 2 points at the CBI-R total scores, both lower than the change in the abnormal groups. The only exception was the MD for the sCC in the *C9orf72* expansion carriers, showing an increase in 3 points at the CDR® plus NACC FTLD total score, similar to the magnitude of change in the abnormal groups. This result might suggest that the clinical progression in presymptomatic *C9orf72* expansion carriers is not related to diffusion measures in sCC, but this has to be confirmed in further cohorts.

In contrast, presymptomatic mutation carriers with regional brain w-scores below the 10th percentile of the controls had significantly worse scores on average after one year. Abnormality on diffusion measures seem to lead to slightly larger significant differences in progression than abnormality in GM volumes, at least for *MAPT* and *C9orf72* mutation carriers for the behavioural scores, whilst the extent of progression was similar between GM and WM regions for *GRN* mutation carriers. One explanation could be that the GM atrophy is slower than WM diffusivity. One study has reported a significant longitudinal rate of change in WM for *MAPT* presymptomatic mutation carriers but not for *C9orf72* and *GRN* mutation carriers.[41]

The results of this study are particularly important when defining biomarkers to stratify participants in future trials. By only using total brain volume, one can predict if *GRN* presymptomatic mutation carriers are likely to progress 3 points on the CDR®+NACC-FTLD sum of boxes score in 12 months. The whole brain volume was not as informative in *C9orf72* expansion carriers, with progression of only 1 point, but this is not surprising probably due to the slow progression of this genetic form, as reported by Staffaroni *et al*.[51] Due to the small number in the subgroups who had abnormal whole brain volume at baseline and available follow-up data, unfortunately the results were inconclusive for *MAPT* mutation carriers and for progression on the CBI-R total score in all three groups. There could be the potential of a 11-16 points increase on the CBI-R total score in *MAPT* and *GRN* presymptomatic mutation carriers with abnormal whole brain volume, but larger studies are needed to confirm this.

However, specific regional measures for each of the genetic forms are associated with a larger increase in clinical scores. For *C9orf72* and *GRN* mutation carriers, both GM and WM tracts were associated with a similar worsening in behavioural symptoms, with a maximum of 8-10 points. *MAPT* mutation carriers showed a maximum of 11 points which showed the potential of being higher in a number of regions (up to 19 points) if this could be confirmed in larger samples. However, in contrast, for the CDR®+NACC-FTLD sum of boxes, both *GRN* and *C9orf72* mutation carriers showed a larger increase compared to *MAPT* mutation carriers (4-5 points vs 2 points, which were not statistically significant). This may be related to differences in the types of clinical features detected by the CDR®+NACC-FTLD in comparison to the CBI-R, with more cognitive and linguistic aspects that are seen in *GRN* and *C9orf72* mutation carriers measured by the CDR.

Despite abnormality on diffusion indexes seeming to be associated with slightly larger changes in clinical scores, abnormality in GM volumes was still associated with a significant change in both the scales used. This is particularly important, as diffusion measures are usually more difficult to obtain than volumes because of higher scanner requirements to acquire the sequences, measurement variability across different scanner types, and the advanced processing required to extract the measures. In addition, diffusion imaging is more prone to image artefacts than conventional T1-weighted structural imaging.

Future studies need to clarify what is a clinically relevant change in such clinical scores, and if the increase predicted by GM volumes are sufficient to discriminate “progressors” vs “non progressors” in the context of clinical trials. Moreover, it will be important to analyse the longitudinal evolution of brain changes and their correlations with the development and onset of symptoms. Another important future investigation is the detailed analyses of which cognitive or behavioural change would be better predicted by abnormal brain features at baseline, and how other variables can contribute to these different profiles of progression. In this study we only focused on the global scores, but a dedicated investigation of the single subscores and specific cognitive domains is needed, including also measures that might predict motor phenotypes, especially for *C9orf72* expansion carriers. Moreover, as these findings are derived from group-level analyses, their relevance and application at the level of the single individual has still to be demonstrated.

This study has some limitations, including the difficulty of investigating small brain nuclei and tracts, which can be only accurately measured with the higher spatial resolution and contrast provided by high field MRI. For this reason, when looking at the progression of clinical and behavioural scores we only focused on the whole structures. Moreover, the MR images were acquired from different scanners: despite the correction for manufacturer, together with other confounding variables, when computing the w-scores, we cannot assume their effects have been fully excluded. Moreover, in subgroups with less than 6 cases the limitations of the Wilcoxon Signed Rank test meant that despite showing large changes these could not reach statistical significance. Further studies with larger samples are important to provide evidence on this matter. Another important study would be to investigate the threshold for abnormality of w-scores by setting the threshold at the 5th percentile, rather than the 10th, to determine if even larger differences are seen over time in these more stringent subgroups. We examined this threshold in the current cohort, but unfortunately the small sample size of the abnormal subgroups prevented further analysis from being possible, and larger samples are needed.

In summary, by looking at *in vivo* regional volumetry, we have quantified and localised regional abnormalities on MRI in presymptomatic and symptomatic mutation carriers, and were able to detect different profiles of clinical and behavioural changes over time from brain abnormalities at baseline. This provides important evidence that imaging biomarkers can be helpful in designing clinical trials at the presymptomatic stages of genetic FTD.

Acknowledgments

We thank the research participants and their families for their contribution to the study.

Funding

The Dementia Research Centre is supported by Alzheimer's Research UK, Alzheimer's Society, Brain Research UK, and The Wolfson Foundation. This work was supported by the National Institute for Health Research (NIHR) Queen Square Dementia Biomedical Research Unit and the University College London Hospitals Biomedical Research Centre, the Leonard Wolfson Experimental Neurology Centre (LWENC) Clinical Research Facility, and the UK Dementia Research Institute, which receives its funding from UK DRI Ltd, funded by the UK Medical Research Council (MRC), Alzheimer's Society and Alzheimer's Research UK. This work was also supported by the MRC UK GENFI grant (MR/M023664/1), the Italian Ministry of Health (CoEN015 and Ricerca Corrente), the Canadian Institutes of Health Research as part of a Centres of Excellence in Neurodegeneration grant, a Canadian Institutes of Health Research operating grant, the Alzheimer's Society grant (AS-PG-16-007), the Bluefield Project and the EU Joint Programme – Neurodegenerative Disease Research (JPND) GENFI-PROX grant (2019-02248). MB is supported by a Fellowship award from the Alzheimer's Society, UK (AS-JF-19a-004-517). MB's work was also supported by the UK Dementia Research Institute which receives its funding from DRI Ltd, funded by the UK Medical Research Council, Alzheimer's Society and Alzheimer's Research UK. MB acknowledges the support of NVIDIA Corporation with the donation of the Titan V GPU used for part of the analyses in this research. JDR is supported by the Miriam Marks Brain Research UK Senior Fellowship and has received funding from an MRC Clinician Scientist Fellowship (MR/M008525/1) and the NIHR Rare Disease Translational Research Collaboration (BRC149/NS/MH). JEI is supported by the European Research Council (Starting Grant 677697, project BUNGEE-TOOLS), Alzheimer's Research UK (ARUK-IRG2019A003) and the NIH (1RF1MH123195-01 and 1R01AG070988-01). JBR is funded by the Wellcome Trust (103838) and the National Institute for Health Research Cambridge Biomedical Research Centre. This work was funded by the Deutsche Forschungsgemeinschaft (DFG, German Research Foundation) under Germany's Excellence Strategy within the framework of the Munich Cluster for Systems Neurology (EXC 2145 SyNergy – ID 390857198). RV's work is supported by the Mady Browaeys Fonds voor Onderzoek naar Frontotemporale Degeneratie. Several authors of this publication (JCvS, MS, RSV, AD, MO, RV, JDR) are members of the European Reference Network for Rare Neurological Diseases (ERN-RND) - Project ID No 739510.

Competing interests

The authors report no competing interest.

Appendix - List of GENFI consortium authors.

Aitana Sogorb Esteve, Annabel Nelson, Carolin Heller, Caroline V. Greaves, Hanya Benotmane, Henrik Zetterberg, Imogen J. Swift, Kiran Samra, Rachelle Shafei, Carolyn Timberlake, Thomas Cope, Timothy Rittman, Alberto Benussi, Enrico Premi, Roberto Gasparotti, Silvana Archetti, Stefano Gazzina, Valentina Cantoni, Andrea Arighi, Chiara Fenoglio, Elio Scarpini, Giorgio Fumagalli, Vittoria Borracci, Giacomina Rossi, Giorgio Giaccone, Giuseppe Di Fede, Paola Caroppo, Pietro Tiraboschi, Sara Prioni, Veronica Redaelli, David Tang-Wai, Ekaterina Rogaeva, Miguel Castelo-Branco, Morris Freedman, Ron Keren, Sandra Black, Sara Mitchell, Christen Shoesmith, Robart Bartha, Rosa Rademakers, Jackie Poos, Janne M. Papma, Lucia Giannini, Rick van Minkelen, Yolande Pijnenburg, Benedetta Nacmias, Camilla Ferrari, Cristina Polito, Gemma Lombardi, Valentina Bessi, Michele Veldsman, Christin Andersson, Hakan Thonberg, Linn Öijerstedt, Vesna Jelic, Paul Thompson, Tobias Langheinrich, Albert Lladó, Anna Antonell, Jaume Olives, Mircea Balasa, Nuria Bargalló, Sergi Borrego-Ecija, Ana Verdelho, Carolina Maruta, Catarina B. Ferreira, Gabriel Miltenberger, Frederico Simões do Couto, Alazne Gabilondo, Ana Gorostidi, Jorge Villanua, Marta Cañada, Mikel Tainta, Miren Zulaica, Myriam Barandiaran, Patricia Alves, Benjamin Bender, Carlo Wilke, Lisa Graf, Annick Vogels, Mathieu Vandenbulcke, Philip Van Damme, Rose Bruffaerts, Koen Poesen, Pedro Rosa-Neto, Serge Gauthier, Agnès Camuzat, Alexis Brice, Anne Bertrand, Aurélie Funkiewiez, Daisy Rinaldi, Dario Saracino, Olivier Colliot, Sabrina Sayah, Catharina Prix, Elisabeth Wlasich, Olivia Wagemann, Sandra Loosli, Sonja Schönecker, Tobias Hoegen, Jolina Lombardi, Sarah Anderl-Straub, Adeline Rollin, Gregory Kuchcinski, Maxime Bertoux, Thibaud Lebouvier, Vincent Deramecourt, Beatriz Santiago, Diana Duro, Maria João Leitão, Maria Rosario Almeida, Miguel Tábuas-Pereira, Sónia Afonso.

References

1. Warren JD, Rohrer JD, Rossor MN. Clinical review. Frontotemporal dementia. BMJ 2013;347:f4827.
2. Rohrer JD, Nicholas JM, Cash DM, van Swieten J, Dopper E, Jiskoot L, et al. Presymptomatic cognitive and neuroanatomical changes in genetic frontotemporal dementia in the Genetic Frontotemporal dementia Initiative (GENFI) study: a cross-sectional analysis. Lancet Neurol. 2015;14(3):253-62.
3. Jiskoot LC, Bocchetta M, Nicholas JM, Cash DM, Thomas D, Modat M, et al. Presymptomatic white matter integrity loss in familial frontotemporal dementia in the GENFI cohort: A cross-sectional diffusion tensor imaging study. Ann Clin Transl Neurol. 2018;5(9):1025-1036.
4. Chen Q, Kantarci K. Imaging Biomarkers for Neurodegeneration in Presymptomatic Familial Frontotemporal Lobar Degeneration. Front Neurol. 2020;11:80.
5. Miyagawa T, Brushaber D, Syrjanen J, Kremers W, Fields J, Forsberg LK, et al. Utility of the global CDR® plus NACC FTLD rating and development of scoring rules: Data from the ARTFL/LEFFTDS Consortium. Alzheimer's & dementia: the journal of the Alzheimer's Association. 2020;16(1):106–117.
6. Wear HJ, Wedderburn CJ, Mioshi E, Williams-Gray CH, Mason SL, Barker RA, et al. The Cambridge Behavioural Inventory revised. Dement Neuropsychol. 2008;2(2):102-107.
7. Bocchetta M, Todd EG, Peakman G, Cash DM, Convery RS, Russell LL, et al. Differential early subcortical involvement in genetic FTD within the GENFI cohort. Neuroimage Clin. 2021;30:102646.
8. Cardoso MJ, Modat M, Wolz R, Melbourne A, Cash D, Rueckert D, et al. Geodesic information flows: spatially-variant graphs and their application to segmentation and fusion. IEEE TMI 2015 doi: 10.1109/TMI.2015.2418298.
9. Iglesias JE, Augustinack JC, Nguyen K, Player CM, Player A, Wright M, et al. A computational atlas of the hippocampal formation using ex vivo, ultra-high resolution MRI: Application to adaptive segmentation of in vivo MRI. Neuroimage. 2015;115:117-137.
10. Iglesias JE, Van Leemput K, Bhatt P, Casillas C, Dutt S, Schuff N, et al. Bayesian segmentation of brainstem structures in MRI. Neuroimage. 2015;113:184-95.
11. Iglesias JE, Insausti R, Lerma-Usabiaga G, Bocchetta M, Van Leemput K, Greve DN, et al. A probabilistic atlas of the human thalamic nuclei combining ex vivo MRI and histology. Neuroimage. 2018.183:314-326.

12. Saygin ZM, Kliemann D, Iglesias JE, van der Kouwe AJW, Boyd E, Reuter M, et al. High-resolution magnetic resonance imaging reveals nuclei of the human amygdala: manual segmentation to automatic atlas. Neuroimage. 2017;155:370-382.
13. Bocchetta M, Iglesias JE, Scelsi MA, Cash DM, Cardoso MJ, Modat M, et al. Hippocampal subfield volumetry: differential pattern of atrophy in different forms of genetic frontotemporal dementia. Journal of Alzheimer's Disease 2018;64(2):497-504.
14. Bocchetta M, Iglesias JE, Cash DM, Warren JD, Rohrer JD. Amygdala subnuclei are differentially affected in the different genetic and pathological forms of frontotemporal dementia. Alzheimer's & Dementia: Diagnosis, Assessment & Disease Monitoring. 2019;11:136-141.
15. Bocchetta M, Iglesias JE, Neason M, Cash DM, Warren JD, Rohrer JD. Thalamic nuclei in frontotemporal dementia: mediodorsal nucleus involvement is universal but pulvinar atrophy is unique to C9orf72. Human Brain Mapping. 2020;41(4):1006-1016.
16. Bocchetta M, Iglesias JE, Chelban V, Jabbari E, Lamb R, et al. Automated brainstem segmentation detects differential involvement in atypical parkinsonian syndromes. Journal of Movement Disorders. 2020;13(1):39-46.
17. Billot B, Bocchetta M, Todd E, Dalca A, Rohrer J, Iglesias Gonzalez JE. Automated segmentation of the Hypothalamus and associated subunits in brain MRI. Neuroimage. 2020:117287, doi: 10.1016/j.neuroimage.2020.117287.
18. Diedrichsen J, Balsters JH, Flavell J, Cussans E, Ramnani N. A probabilistic MR atlas of the human cerebellum. NeuroImage. 2009;46(1):39-46.
19. Diedrichsen J, Maderwald S, Küper M, Thürling M, Rabe K, Gizewski ER, et al. Imaging the deep cerebellar nuclei: a probabilistic atlas and normalization procedure. NeuroImage 2011;54(3):1786-1794.
20. Malone IB, Leung KK, Clegg S, Barnes J, Whitwell JL, Ashburner J, et al. Accurate automatic estimation of total intracranial volume: a nuisance variable with less nuisance. Neuroimage. 2015;104:366-72.
21. Jenkinson M. FSL. NeuroImage. 2012;62:782–790.
22. Andersson JLR, Sotiropoulos SN. An integrated approach to correction for off-resonance effects and subject movement in diffusion MR imaging. Neuroimage. 2016;125:1063-1078.

23. Daga P, Pendse T, Modat M, White M, Mancini L, Winston GP, et al. Susceptibility artefact correction using dynamic graph cuts: application to neurosurgery. Med Image Anal. 2014;18(7):1132-42.

24. Melbourne A, Toussaint N, Owen D, Simpson I, Anthopoulos T, De Vita E, et al. NiftyFit: a Software Package for Multi-parametric Model-Fitting of 4D Magnetic Resonance Imaging Data. Neuroinformatics. 2016;14(3):319-37.

25. Zhang H, Yushkevich P, Alexander D, Gee J. Deformable registration of diffusion tensor MR images with explicit orientation optimization. Med Image Anal 2006;10:764–785.

26. Zhang Y, Schuff N, Jahng GH, Bayne W, Mori S, Schad L, et al. Diffusion tensor imaging of cingulum fibers in mild cognitive impairment and Alzheimer disease. Neurology. 2007;68(1):13-9.

27. Zhang Y, Schuff N, Du AT, Rosen HJ, Kramer JH, Gorno-Tempini ML, Miller BL, Weiner MW. White matter damage in frontotemporal dementia and Alzheimer's disease measured by diffusion MRI. Brain. 2009;132(Pt 9):2579-92.

28. Wang Y, Gupta A, Liu Z, Zhang H, Escolar ML, Gilmore JH, et al. DTI registration in atlas based fiber analysis of infantile Krabbe disease. Neuroimage. 2011;55(4):1577-86.

29. Keihaninejad S, Zhang H, Ryan NS, Malone IB, Modat M, Cardoso MJ, Cash DM, Fox NC, Ourselin S. An unbiased longitudinal analysis framework for tracking white matter changes using diffusion tensor imaging with application to Alzheimer's disease. Neuroimage. 2013;72:153-63.

30. Yushkevich PA, Zhang H, Simon TJ, Gee JC. Structure-specific statistical mapping of white matter tracts. Neuroimage. 2008;41(2):448-61.

31. Zhang H, Awate SP, Das SR, Woo JH, Melhem ER, Gee JC, et al. A tract-specific framework for white matter morphometry combining macroscopic and microscopic tract features. Med Image Anal. 2010;14(5):666-73.

32. Zhang H, Yushkevich PA, Rueckert D, Gee JC. A computational white matter atlas for aging with surface-based representation of fasciculi. 2010. In International Workshop on Biomedical Image Registration, volume 6204 of Lecture Notes in Computer Science, pages 83-90.

33. Zhang H, Avants BB, Yushkevich PA, Woo JH, Wang S, McCluskey LF, et al. High-dimensional spatial normalization of diffusion tensor images improves the detection of white matter differences: an example study using amyotrophic lateral sclerosis. IEEE Trans Med Imaging. 2007;26(11):1585-97.

34. Modat M, Ridgway GR, Taylor ZA, Lehmann M, Barnes J, Hawkes DJ, Fox NC, Ourselin Set al. Fast free-form deformation using graphics processing units. Comput Methods Programs Biomed. 2010;98(3):278-84.
35. Wakana S, Caprihan A, Panzenboeck MM, Fallon JH, Perry M, Gollub RL, et al. Reproducibility of quantitative tractography methods applied to cerebral white matter. Neuroimage. 2007;36(3):630-44.
36. Lee SE, Sias AC, Mandelli ML, Brown JA, Brown AB, Khazenzon AM, et al. Network degeneration and dysfunction in presymptomatic C9ORF72 expansion carriers. Neuroimage Clin. 2016;14:286-297.
37. Convery RS, Bocchetta M, Greaves CV, Moore KM, Cash DM, Van Swieten J, et al. Abnormal pain perception is associated with thalamo-cortico-striatal atrophy in C9orf72 expansion carriers in the GENFI cohort. J Neurol Neurosurg Psychiatry. 2020:jnnp-2020-323279.
38. Ducharme S, Bajestan S, Dickerson BC, Voon V. Psychiatric presentations of C9orf72 mutation: What are the diagnostic implications for clinicians? Journal of Neuropsychiatry and Clinical Neurosciences. 2017;29(3),195–205.
39. Fletcher PD, Downey LE, Golden HL, Clark CN, Slattery CF, Paterson RW, et al. Pain and temperature processing in dementia: A clinical and neuroanatomical analysis. Brain 2015; 138(Pt 11):3360–3372.
40. Kertesz A, Ang LC, Jesso S, MacKinley J, Baker M, Brown P, et al. Psychosis and hallucinations in frontotemporal dementia with the C9ORF72 mutation: a detailed clinical cohort. Cogn Behav Neurol. 2013;26(3):146-54.
41. Panman JL, Jiskoot LC, Bouts MJRJ, Meeter LHH, van der Ende EL, Poos JM, et al. Gray and white matter changes in presymptomatic genetic frontotemporal dementia: a longitudinal MRI study. Neurobiol Aging. 2019;76:115-124.
42. Bertrand A, Wen J, Rinaldi D, Houot M, Sayah S, Camuzat A, et al. Early Cognitive, Structural, and Microstructural Changes in Presymptomatic C9orf72 Carriers Younger Than 40 Years. JAMA Neurol. 2018;75(2):236-245.
43. Whitwell JL, Weigand SD, Boeve BF, Senjem ML, Gunter JL, DeJesus-Hernandez M, et al. Neuroimaging signatures of frontotemporal dementia genetics: C9ORF72, tau, progranulin and sporadics. Brain. 2012;135(Pt 3):794-806.
44. Menon V. Salience Network. 2015. In: Arthur W. Toga, editor. Brain Mapping: An Encyclopedic Reference, vol. 2, pp. 597-611. Academic Press: Elsevier.

45. Chen Q, Boeve BF, Schwarz CG, Reid R, Tosakulwong N, Lesnick TG, et al. Tracking white matter degeneration in asymptomatic and symptomatic MAPT mutation carriers. Neurobiol Aging. 2019;83:54-62.
46. Dopper EG, Rombouts SA, Jiskoot LC, Heijer T, de Graaf JR, Koning I, et al. Structural and functional brain connectivity in presymptomatic familial frontotemporal dementia. Neurology. 2013;80(9):814-23.
47. Olm CA, McMillan CT, Irwin DJ, Van Deerlin VM, Cook PA, Gee JC, et al. Longitudinal structural gray matter and white matter MRI changes in presymptomatic progranulin mutation carriers. Neuroimage Clin. 2018;19:497-506.
48. Sudre CH, Bocchetta M, Cash D, Thomas DL, Woollacott I, Dick KM, et al. White matter hyperintensities are seen only in GRN mutation carriers in the GENFI cohort. Neuroimage Clin. 2017;15:171-180.
49. Jiskoot LC, Panman JL, Meeter LH, Dopper EGP, Donker Kaat L, Franzen S, et al. Longitudinal multimodal MRI as prognostic and diagnostic biomarker in presymptomatic familial frontotemporal dementia. Brain. 2019;142(1):193-208.
50. Warren JD, Rohrer JD, Schott JM, Fox NC, Hardy J, Rossor MN. Molecular nexopathies: a new paradigm of neurodegenerative disease. Trends Neurosci. 2013;36(10):561-9.
51. Staffaroni AM, Goh SM, Cobigo Y, Ong E, Lee SE, Casaletto KB, et al. Rates of Brain Atrophy Across Disease Stages in Familial Frontotemporal Dementia Associated With MAPT, GRN, and C9orf72 Pathogenic Variants. JAMA Netw Open. 2020;3(10):e2022847.

Figure Legends

Figure 1. **Regions of interest used in the grey and white matter analyses.** Abbreviations. Cortex: VMPFC ventromedial prefrontal, TP temporal pole, MT medial temporal, CING cingulate, MOT motor, S sensory, MP medial parietal, OCC occipital, DLPFC dorsolateral prefrontal, OF orbitofrontal, INS insula, DLT dorsolateral temporal, LP lateral parietal; Basal ganglia and Basal forebrain: GP pallidum, CAU caudate, PUT putamen, BF basal forebrain, NA nucleus accumbens; Brainstem and Cerebellum: SCP superior cerebellar peduncle, MB midbrain, ME medulla; VIIA – CI lobule VIIA – Crus I, VIIA – CII lobule VIIA – Crus II, DN deep nuclei; Amygdala: CAT cortico-amygdaloid transition area, Sup superficial nuclei, AB accessory basal nucleus; Hippocampus: DG dentate gyrus, CA cornu ammonis; Thalamus: AV anteroventral, VA ventral anterior, LD laterodorsal, VLa ventral lateral anterior, MD mediodorsal, LP lateral posterior, VLp ventral lateral posterior, VPL ventral posterolateral, VM ventromedial, LGN lateral geniculate nucleus, MGN medial geniculate nucleus; Hypothalamus: as anterior superior, ai anterior inferior, s-tub superior tuberal, i-tub inferior tuberal, pos posterior; White matter tracts: UF uncinate fasciculus, SLF superior longitudinal fasciculus, Cing cingulum, SS sagittal stratum, pTR posterior thalamic radiation, aCR anterior corona radiata, pCR posterior corona radiata, sCR superior corona radiata, EC external capsule, aIC anterior part of the internal capsule, pIC posterior part of the internal capsule, rIC retrolenticular part of the internal capsule, gCC genu of the corpus callosum, bCC body of the corpus callosum, sCC splenium of the corpus callosum.

Figure 2. **Pattern of grey matter involvement in *C9orf72* for the stages defined by CDR®+NACC FTLD global scores.** The colour map indicates the percentile corresponding to the mean w-scores in each group (*C9orf72* ≤0.5/≥1), when these were statistically abnormal (i.e., significantly different from 0, t-test) when compared to controls (n=240).

Figure 3. **Pattern of grey matter involvement in *MAPT* for the stages defined by CDR®+NACC FTLD global scores.** The colour map indicates the percentile corresponding to the mean w-scores in each group (*MAPT* ≤0.5/≥1: n=52/15), when these were statistically abnormal (i.e., significantly different from 0, t-test) when compared to controls (n=240).

Figure 4. **Pattern of grey matter involvement in *GRN* for the stages defined by CDR®+NACC FTLD global scores.** The colour map indicates the percentile corresponding to the mean w-scores in each group (*GRN* ≤0.5/≥1: n=130/30), when these were statistically abnormal (i.e., significantly different from 0, t-test) when compared to controls (n=240).

Figure 5. **Pattern of white matter involvement in *C9orf72* for the stages defined by CDR®+NACC FTLD global scores.** FA indexes are reported on the left side of the figure, while MD on the right. The colour map indicates the percentile corresponding to the mean w-scores in each group (*C9orf72* ≤0.5/≥1: n=113/47), when these were statistically abnormal (i.e., significantly different from 0, t-test) when compared to controls (n=240).

Figure 6. **Pattern of white matter involvement in *MAPT* for the stages defined by CDR®+NACC FTLD global scores.** FA indexes are reported on the left side of the figure, while MD on the right. The colour map indicates the percentile corresponding to the mean w-scores in each group (*MAPT* ≤0.5/≥1: n=52/15), when these were statistically abnormal (i.e., significantly different from 0, t-test) when compared to controls (n=240).

Figure 7. **Pattern of white matter involvement in *GRN* for the stages defined by CDR®+NACC FTLD global scores.** FA indexes are reported on the left side of the figure, while MD on the right. The colour map indicates the percentile corresponding to the mean w-scores in each group (*GRN* ≤0.5/≥1: n=130/30), when these were statistically abnormal (i.e., significantly different from 0, t-test) when compared to controls (n=240).

Figure 8. **Longitudinal changes in the CDR®+NACC FTLD sum of boxes scores (first row) and CBI-R total scores (second row) in the presymptomatic mutation carriers for those with w-scores of the whole brain volume above ("normal" in black) and below ("abnormal" in red) the 10th percentile of the controls.** Asterisks indicate a significant difference in progression between visits within the two groups at Wilcoxon Signed Rank exact test (p≤0.05). Bars indicate the 95% confidence intervals of the mean. Analyses were performed on: *C9orf72* n=56; *MAPT* n=32; *GRN* n=69.

Figure 9. **Largest longitudinal changes in the CDR®+NACC FTLD sum of boxes scores (first row) and CBI-R total scores (second row) in the presymptomatic mutation carriers for those with "normal" and "abnormal" w-scores for GM and WM regions.** Y-axis represents estimated marginalised means**.** Asterisks indicate a significant difference in progression between visits within the two groups at Wilcoxon Signed Rank exact test (p≤0.05). Bars indicate the 95% confidence intervals of the mean. Analyses were performed on: *C9orf72* n=56; *MAPT* n=32; *GRN* n=69. Abbreviations. DLPFC dorsolateral prefrontal, VMPFC ventromedial prefrontal, MED PARIETAL medial parietal, FA fractional

anisotropy, MD mean diffusivity, UF uncinate fasciculus, SS sagittal stratum, gCC genu of the corpus callosum, sCR superior corona radiata, aCR anterior corona radiata.

Table 1: Demographic and clinical characteristic of the cohort divided by genetic group and CDR®+NACC FTLD global scores. Abbreviations: SD standard deviation, N/A not applicable, N/I not included in the analyses, FTD frontotemporal dementia, bvFTD behavioural variant FTD, PPA primary progressive aphasia, NOS not otherwise specified, CBS corticobasal syndrome, PSP progressive supranuclear palsy, ALS amyotrophic lateral sclerosis, CBI-R revised version of the Cambridge Behavioural Inventory.

	Non-carriers	***C9orf72* expansion carriers**		***MAPT* mutation carriers**		***GRN* mutation carriers**	
CDR®+NACC FTLD global score		**≤0.5**	**≥1**	**≤0.5**	**≥1**	**≤0.5**	**≥1**
N	240	113	47	52	15	130	30
Age, year (mean and SD)	44.8(12.2)	45.0(11.5)	63.5(7.4)	41.1(10.6)	59.2(9.3)	46.5(12.2)	63.3(8.1)
Sex, male (%)	103(42.9%)	48(42.5%)	31(66.0%)	21(40.4%)	9(60.0%)	48(36.9%)	14(46.7%)
Clinical phenotype	N/A	N/A	36 bvFTD, 4 FTD-ALS, 2 ALS, 2 PPA, 1 PSP, 1 Dementia-NOS, 1 Other	N/A	13 bvFTD, 1 PPA, 1 Dementia-NOS	N/A	16 bvFTD, 12 PPA, 1 CBS, 1 Other
CDR®+NACC FTLD sum of boxes score (mean and SD) (baseline/follow-up)	N/A	0.2(0.5)/0.9(2.5)	N/I	0.3(0.7)/0.6(1.3)	N/I	0.2(0.5)/0.8(2.8)	N/I

CBI-R total score (mean and SD) (baseline/follow-up)	N/A	9.0(9.5)/9.4(14.5)	N/I	6.8(7.8)/9.0(13.4)	N/I	5.2(8.5)/7.0(13.5)	N/I

Supplementary table legends

In case of formatting issues, the Supplementary Tables can be downloaded here: www.dropbox.com/s/40wjebpxpc4h331/Bocchetta_Suppl_Tables.xlsx?dl=0

Supplementary Table 1. Overview of MRI scanners and acquisition parameters. Abbreviations: GE General Electric; FOV field of view; TI inversion time; TR repetition time; TE echo time; FM field map; EPI echo-planar imaging; PE phase-encoding; AP anterior-posterior.

Supplementary Table 2: Grey matter regions for *C9orf72*, *MAPT* and *GRN* for the stages defined by CDR®+NACC FTLD global scores. Values denote mean and standard deviation (SD) for the w-scores. Bold indicates significantly negative w-scores after Bonferroni correction for multiple comparisons. Abbreviations. Cortex: DLPFC dorsolateral prefrontal, VMPFC ventromedial prefrontal; Brainstem and Cerebellum: SCP superior cerebellar peduncle; VIIA – CI lobule VIIA – Crus I, VIIA – CII lobule VIIA – Crus II, DN deep nuclei; Amygdala: CAT cortico-amygdaloid transition area, Sup superficial nuclei, AB accessory basal nucleus; Hippocampus: DG dentate gyrus, CA cornu ammonis; Thalamus: AV anteroventral, VA ventral anterior, LD laterodorsal, VLa ventral lateral anterior, MD mediodorsal, LP lateral posterior, VLp ventral lateral posterior, VPL ventral posterolateral, VM ventromedial, LGN lateral geniculate nucleus, MGN medial geniculate nucleus; Hypothalamus: as anterior superior, ai anterior inferior, s-tub superior tuberal, i-tub inferior tuberal.

Supplementary Table 3: White matter regions for *C9orf72*, *MAPT* and *GRN* for the stages defined by CDR®+NACC FTLD global scores. Values denote mean and standard deviation (SD) for the w-scores in the fractional anisotropy (FA) and mean diffusivity (MD). Bold indicates significantly negative w-scores after Bonferroni correction for multiple comparisons. Abbreviations. UF uncinate fasciculus, SLF superior longitudinal fasciculus, SS sagittal stratum, pTR posterior thalamic radiation, aCR anterior corona radiata, pCR posterior corona radiata, sCR superior corona radiata, EC external capsule, aIC anterior part of the internal capsule, pIC posterior part of the internal capsule, rIC retrolenticular part of the internal capsule, gCC genu of the corpus callosum, bCC body of the corpus callosum, sCC splenium of the corpus callosum.

Supplementary Table 4: Longitudinal progression at the CDR®+NACC FTLD sum of boxes scores for the "normal" and "abnormal" groups for each of the ROIs in the *C9orf72*, *MAPT* and *GRN* presymptomatic carriers. Red indicates

significantly difference in time. Abbreviations. FA fractional anisotropy, MD mean diffusivity, SD standard deviation, Diff mean difference between the two visits, 95% CI 95% confidence interval of the mean difference, DLPFC dorsolateral prefrontal, VMPFC ventromedial prefrontal, UF uncinate fasciculus, SLF superior longitudinal fasciculus, SS sagittal stratum, pTR posterior thalamic radiation, aCR anterior corona radiata, pCR posterior corona radiata, sCR superior corona radiata, EC external capsule, aIC anterior part of the internal capsule, pIC posterior part of the internal capsule, rIC retrolenticular part of the internal capsule, gCC genu of the corpus callosum, bCC body of the corpus callosum, sCC splenium of the corpus callosum.

Supplementary Table 5: Longitudinal progression at the CBI-R total scores for the "normal" and "abnormal" groups for each of the ROIs in the *C9orf72*, *MAPT* and *GRN* presymptomatic carriers. Red indicates significantly difference in time. Abbreviations. FA fractional anisotropy, MD mean diffusivity, SD standard deviation, Diff mean difference between the two visits, 95% CI 95% confidence interval of the mean difference, DLPFC dorsolateral prefrontal, VMPFC ventromedial prefrontal, UF uncinate fasciculus, SLF superior longitudinal fasciculus, SS sagittal stratum, pTR posterior thalamic radiation, aCR anterior corona radiata, pCR posterior corona radiata, sCR superior corona radiata, EC external capsule, aIC anterior part of the internal capsule, pIC posterior part of the internal capsule, rIC retrolenticular part of the internal capsule, gCC genu of the corpus callosum, bCC body of the corpus callosum, sCC splenium of the corpus callosum.

Supplementary Material: Detailed description of the results from the GM and WM analyses at baseline.

Baseline GM volumes

At the presymptomatic stage, *C9orf72* expansion carriers had significantly lower w-scores in all the cortical regions except for the VMPFC, medial temporal and orbitofrontal cortex (**Figure 2**, **Supplementary Table 2**). Among the subcortical regions, the putamen and globus pallidus had significantly lower volumes, together with the lobule V, VI, VIIa-Crus II, VIIb and VIIIb of the cerebellum. The amygdala and hippocampus also had significantly lower volumes (except for the hippocampal tail and subiculum), as did the s-tub region of the hypothalamus. The thalamus was the structure with the most abnormal regions: the pulvinar had values below the 10th percentile of the controls, and the mediodorsal, anteroventral, ventral anterior, ventral lateral anterior, lateral posterior and LGN had values below the 25th percentile (**Figure 2**, **Supplementary Table 2**). Only the ventromedial thalamic region was not significantly smaller than controls. At the fully symptomatic stage, *C9orf72* expansion carriers had significantly lower w-scores in all the cortical regions, with values below the 2.5th percentile in the insula and dorsolateral temporal cortex (**Figure 2**, **Supplementary Table 2**), and below the 5th percentile in the DLPFC, motor and lateral parietal, and below the 10th percentile in the orbitofrontal cortex. The putamen and globus pallidus had values <5th and <10th percentile respectively, and the cerebellum had significantly lower values (<25th percentile) in the VIIIa and VIIIb, and in the I-IV, VI, VIIa-Crus II, VIIb and vermis (>25th percentile). The amygdalar and hippocampal regions were all below the 2.5th percentile, except for the lateral amygdala, presubiculum and subiculum (<5th percentile) and hippocampal tail (<10th percentile). The hypothalamus had values <10th percentile in the anterior-superior, s-tub and posterior, and <25th percentile in the anterior-inferior. Finally, all the thalamic regions were affected, with values <2.5th percentile in the mediodorsal and anteroventral, <5th percentile in the lateral posterior and pulvinar, <10th percentile in the midline, intralaminar and LD, <25th percentile in the ventral anterior, ventral lateral anterior, ventral lateral posterior and LGN.

At the presymptomatic stage, *MAPT* mutation carriers had significantly lower w-scores in the dorsolateral temporal cortex, but not in other cortical, cerebellar or brainstem regions (**Figure 2**, **Supplementary Table 2**). All regions of the amygdala were significantly lower than controls (except for the lateral region), with the accessory basal nucleus showing values <25th percentile. The subiculum and presubiculum were also significantly lower, together with the LGN in the thalamus. When fully symptomatic, *MAPT* mutation carriers showed extremely low values (<2.5th percentile) in all the temporal cortex,

amygdala, hippocampus and insula. The cingulate (<25th percentile) and orbitofrontal cortex were also significantly lower (**Figure 2**, **Supplementary Table 2**). The values of the nucleus accumbens, globus pallidus, and midbrain were all below the 25th percentile, while the putamen values were below the 10th. The hypothalamus showed values <2.5th percentile in the anterior-superior, s-tub and posterior, <10th in the anterior-inferior, and <25th in the i-tub. All the thalamic regions (except for the LGN) were significantly lower than the 25th percentile, with the mediodorsal values <5th and the anteroventral values <10th percentile.

Presymptomatic *GRN* mutation carriers showed significantly lower values in the temporal pole, presubiculum, and in the anterior superior cerebellum (lobule I-IV, V and VI). No other brain region was affected in this early stage (**Figure 2**, **Supplementary Table 2**). Fully symptomatic *GRN* mutation carriers showed significantly lower volumes in all cortical regions, except for the sensory cortex, with extremely low w-scores (<2.5th percentile) in the DLPFC, insula and motor cortex, values <5th percentile in the dorsolateral temporal and lateral parietal cortex, <10th in the cingulate and orbitofrontal cortex, and <25th in the VMPFC, temporal pole, medial parietal and occipital cortex. The w-scores of the globus pallidus and the putamen were below the 25th and 5th percentile respectively, while among the brainstem and cerebellar regions, the midbrain and lobule VIIb were below the 25th percentile, while the pons, lobule VIIa-Crus I, VIIa-Crus II, VIIIa and VIIIb were also significantly lower than control distribution. All amygdalar and hippocampal regions were significantly lower than the 25th percentile, with the lowest values in the presubiculum (<2.5th), accessory basal nucleus (<5th), basal and paralaminar nucleus, cortico-amygdaloid transition area, superficial nuclei, CA1, CA2/CA3, CA4, dentate gyrus, and subiculum (<10th percentile). All the thalamic regions (except for the LGN) were significantly lower than the controls, with the mediodorsal values <2.5th percentile, the midline, anteroventral and ventral anterior values <5th percentile, the lateral posterior and ventral lateral anterior values <10th percentile, and LD, intralaminar, ventromedial, ventral posterolateral and ventral lateral posterior values <25th percentile. The posterior hypothalamus showed values <2.5th percentile, the anterior-superior and s-tub <10th, and anterior-inferior <25th percentile.

Baseline diffusion WM indices

Presymptomatic *C9orf72* expansion carriers showed FA values lower than controls in the SS, whole corpus callosum, pTR, aCR, EC, and aIC (**Figure 3**, **Supplementary Table 3**). MD values were higher than controls in the SS, gCC and sCC, pTR, aCR, pCR, EC, cingulum, and SLF. Symptomatic *C9orf72* expansion carriers showed FA values lower than controls

in all WM tracts except the sCR (not significant), with particularly lower values in the gCC and aCR (<2.5th percentile), aIC, SS, and bCC (<5th percentile), UF, sCC and cingulum (<10th percentile). MD values were <10th percentile in all tracts, expect for the pIC (<25th percentile), with particularly abnormal values (<2.5th percentile) in the SS, corpus callosum (genu and body), aCR, sCR, cingulum, pTR, and aIC (**Figure 3**, **Supplementary Table 3**).

Presymptomatic *MAPT* mutation carriers only showed significantly lower FA than controls in the aIC (**Figure 3**, **Supplementary Table 3**). Once symptoms were present, *MAPT* mutation carriers showed FA values <2.5th percentile for the UF, <10th percentile in the gCC and cingulum, <25th percentile in the SS, aCR and SLF, and significantly lower values in the pTR. MD values were significantly <2.5th percentile of controls in the UF and SS, <5th percentile in the aCR and <10th in the gCC.

At a presymptomatic stage, *GRN* mutation carriers showed significantly lower FA than controls in the sCR, and significantly higher MD than controls in the UF and aCR (**Figure 3**, **Supplementary Table 3**). Fully symptomatic *GRN* mutation carriers showed abnormal FA and MD values in all tracts (**Figure 3**, **Supplementary Table 3**). FA values were <2.5th percentile in the corpus callosum (genu and body), cingulum, aIC, and aCR; <5th percentile in the UF, SS, EC, SLF and sCC. Interestingly, nearly all tracts showed MD values <2.5th percentile, except for the sCC (<5th percentile), UF (<10th percentile), pIC and rIC (<25th percentile) (**Figure 3**, **Supplementary Table 3**).

Appendix

List of GENFI consortium authors:

Author	Affiliation
Aitana Sogorb Esteve	Department of Neurodegenerative Disease, Dementia Research Centre, UCL Queen Square Institute of Neurology, London, UK; UK Dementia Research Institute at University College London, UCL Queen Square Institute of Neurology, London, UK
Annabel Nelson	Department of Neurodegenerative Disease, Dementia Research Centre, UCL Queen Square Institute of Neurology, London, UK
Carolin Heller	Department of Neurodegenerative Disease, Dementia Research Centre, UCL Queen Square Institute of Neurology, London, UK
Caroline V. Greaves	Department of Neurodegenerative Disease, Dementia Research Centre, UCL Queen Square Institute of Neurology, London, UK
Hanya Benotmane	UK Dementia Research Institute at University College London, UCL Queen Square Institute of Neurology, London, UK
Henrik Zetterberg	UK Dementia Research Institute at University College London, UCL Queen Square Institute of Neurology, London, UK; Department of Psychiatry and Neurochemistry, the Sahlgrenska Academy at the University of Gothenburg, Mölndal, Sweden
Imogen J Swift	Department of Neurodegenerative Disease, Dementia Research Centre, UCL Queen Square Institute of Neurology, London, UK; UK Dementia Research Institute at University College London, UCL Queen Square Institute of Neurology, London, UK
Kiran Samra	Department of Neurodegenerative Disease, Dementia Research Centre, UCL Queen Square Institute of Neurology, London, UK
Rachelle Shafei	Department of Neurodegenerative Disease, Dementia Research Centre, UCL Queen Square Institute of Neurology, London, UK
Carolyn Timberlake	Department of Clinical Neurosciences, University of Cambridge, Cambridge, UK
Thomas Cope	Department of Clinical Neuroscience, University of Cambridge, Cambridge, UK
Timothy Rittman	Department of Clinical Neurosciences, University of Cambridge, Cambridge, UK
Alberto Benussi	Centre for Neurodegenerative Disorders, Department of Clinical and Experimental Sciences, University of Brescia, Brescia, Italy
Enrico Premi	Stroke Unit, ASST Brescia Hospital, Brescia, Italy
Roberto Gasparotti	Neuroradiology Unit, University of Brescia, Brescia, Italy
Silvana Archetti	Biotechnology Laboratory, Department of Diagnostics, ASST Brescia Hospital, Brescia, Italy
Stefano Gazzina	Neurology, ASST Brescia Hospital, Brescia, Italy
Valentina Cantoni	Centre for Neurodegenerative Disorders, Department of Clinical and Experimental Sciences, University of Brescia, Brescia, Italy
Andrea Arighi	Fondazione IRCCS Ca' Granda Ospedale Maggiore Policlinico, Neurodegenerative Diseases Unit, Milan, Italy; University of Milan, Centro Dino Ferrari, Milan, Italy
Chiara Fenoglio	Fondazione IRCCS Ca' Granda Ospedale Maggiore Policlinico, Neurodegenerative Diseases Unit, Milan, Italy; University of Milan, Centro Dino Ferrari, Milan, Italy
Elio Scarpini	Fondazione IRCCS Ca' Granda Ospedale Maggiore Policlinico, Neurodegenerative Diseases Unit, Milan, Italy; University of Milan, Centro Dino Ferrari, Milan, Italy

Giorgio Fumagalli	Fondazione IRCCS Ca' Granda Ospedale Maggiore Policlinico, Neurodegenerative Diseases Unit, Milan, Italy; University of Milan, Centro Dino Ferrari, Milan, Italy
Vittoria Borracci	Fondazione IRCCS Istituto Neurologico Carlo Besta, Milano, Italy
Giacomina Rossi	Fondazione IRCCS Istituto Neurologico Carlo Besta, Milano, Italy
Giorgio Giaccone	Fondazione IRCCS Istituto Neurologico Carlo Besta, Milano, Italy
Giuseppe Di Fede	Fondazione IRCCS Istituto Neurologico Carlo Besta, Milano, Italy
Paola Caroppo	Fondazione IRCCS Istituto Neurologico Carlo Besta, Milano, Italy
Pietro Tiraboschi	Fondazione IRCCS Istituto Neurologico Carlo Besta, Milano, Italy
Sara Prioni	Fondazione IRCCS Istituto Neurologico Carlo Besta, Milano, Italy
Veronica Redaelli	Fondazione IRCCS Istituto Neurologico Carlo Besta, Milano, Italy
David Tang-Wai	The University Health Network, Krembil Research Institute, Toronto, Canada
Ekaterina Rogaeva	Tanz Centre for Research in Neurodegenerative Diseases, University of Toronto, Toronto, Canada
Miguel Castelo-Branco	Faculty of Medicine, University of Coimbra, Coimbra, Portugal
Morris Freedman	Baycrest Health Sciences, Rotman Research Institute, University of Toronto, Toronto, Canada
Ron Keren	The University Health Network, Toronto Rehabilitation Institute, Toronto, Canada
Sandra Black	Sunnybrook Health Sciences Centre, Sunnybrook Research Institute, University of Toronto, Toronto, Canada
Sara Mitchell	Sunnybrook Health Sciences Centre, Sunnybrook Research Institute, University of Toronto, Toronto, Canada
Christen Shoesmith	Department of Clinical Neurological Sciences, University of Western Ontario, London, Ontario, Canada
Robart Bartha	Department of Medical Biophysics, The University of Western Ontario, London, Ontario, Canada; Centre for Functional and Metabolic Mapping, Robarts Research Institute, The University of Western Ontario, London, Ontario, Canada
Rosa Rademakers	Center for Molecular Neurology, University of Antwerp
Jackie Poos	Department of Neurology, Erasmus Medical Center, Rotterdam, Netherlands
Janne M. Papma	Department of Neurology, Erasmus Medical Center, Rotterdam, Netherlands
Lucia Giannini	Department of Neurology, Erasmus Medical Center, Rotterdam, Netherlands
Rick van Minkelen	Department of Clinical Genetics, Erasmus Medical Center, Rotterdam, Netherlands
Yolande Pijnenburg	Amsterdam University Medical Centre, Amsterdam Vumc, Amsterdam, Netherlands

Benedetta Nacmias	Department of Neuroscience, Psychology, Drug Research and Child Health, University of Florence, Florence, Italy
Camilla Ferrari	Department of Neuroscience, Psychology, Drug Research and Child Health, University of Florence, Florence, Italy
Cristina Polito	Department of Biomedical, Experimental and Clinical Sciences “Mario Serio”, Nuclear Medicine Unit, University of Florence, Florence, Italy
Gemma Lombardi	Department of Neuroscience, Psychology, Drug Research and Child Health, University of Florence, Florence, Italy
Valentina Bessi	Department of Neuroscience, Psychology, Drug Research and Child Health, University of Florence, Florence, Italy
Michele Veldsman	Nuffield Department of Clinical Neurosciences, Medical Sciences Division, University of Oxford, Oxford, UK
Christin Andersson	Department of Clinical Neuroscience, Karolinska Institutet, Stockholm, Sweden
Hakan Thonberg	Center for Alzheimer Research, Division of Neurogeriatrics, Karolinska Institutet, Stockholm, Sweden
Linn Öijerstedt	Center for Alzheimer Research, Division of Neurogeriatrics, Department of Neurobiology, Care Sciences and Society, Bioclinicum, Karolinska Institutet, Solna, Sweden; Unit for Hereditary Dementias, Theme Aging, Karolinska University Hospital, Solna, Sweden
Vesna Jelic	Division of Clinical Geriatrics, Karolinska Institutet, Stockholm, Sweden
Paul Thompson	Division of Neuroscience and Experimental Psychology, Wolfson Molecular Imaging Centre, University of Manchester, Manchester, UK
Tobias Langheinrich	Division of Neuroscience and Experimental Psychology, Wolfson Molecular Imaging Centre, University of Manchester, Manchester, UK; Manchester Centre for Clinical Neurosciences, Department of Neurology, Salford Royal NHS Foundation Trust, Manchester, UK
Albert Lladó	Alzheimer’s disease and Other Cognitive Disorders Unit, Neurology Service, Hospital Clínic, Barcelona, Spain
Anna Antonell	Alzheimer’s disease and Other Cognitive Disorders Unit, Neurology Service, Hospital Clínic, Barcelona, Spain
Jaume Olives	Alzheimer’s disease and Other Cognitive Disorders Unit, Neurology Service, Hospital Clínic, Barcelona, Spain
Mircea Balasa	Alzheimer’s disease and Other Cognitive Disorders Unit, Neurology Service, Hospital Clínic, Barcelona, Spain
Nuria Bargalló	Imaging Diagnostic Center, Hospital Clínic, Barcelona, Spain
Sergi Borrego-Ecija	Alzheimer’s disease and Other Cognitive Disorders Unit, Neurology Service, Hospital Clínic, Barcelona, Spain
Ana Verdelho	Department of Neurosciences and Mental Health, Centro Hospitalar Lisboa Norte - Hospital de Santa Maria & Faculty of Medicine, University of Lisbon, Lisbon, Portugal
Carolina Maruta	Laboratory of Language Research, Centro de Estudos Egas Moniz, Faculty of Medicine, University of Lisbon, Lisbon, Portugal
Catarina B. Ferreira	Laboratory of Neurosciences, Faculty of Medicine, University of Lisbon, Lisbon, Portugal
Gabriel Miltenberger	Faculty of Medicine, University of Lisbon, Lisbon, Portugal

Frederico Simões do Couto	Faculdade de Medicina, Universidade Católica Portuguesa
Alazne Gabilondo	Cognitive Disorders Unit, Department of Neurology, Donostia University Hospital, San Sebastian, Gipuzkoa, Spain; Neuroscience Area, Biodonostia Health Research Insitute, San Sebastian, Gipuzkoa, Spain
Ana Gorostidi	Neuroscience Area, Biodonostia Health Research Institute, San Sebastian, Gipuzkoa, Spain
Jorge Villanua	OSATEK, University of Donostia, San Sebastian, Gipuzkoa, Spain
Marta Cañada	CITA Alzheimer, San Sebastian, Gipuzkoa, Spain
Mikel Tainta	Neuroscience Area, Biodonostia Health Research Insitute, San Sebastian, Gipuzkoa, Spain
Miren Zulaica	Neuroscience Area, Biodonostia Health Research Insitute, San Sebastian, Gipuzkoa, Spain
Myriam Barandiaran	Cognitive Disorders Unit, Department of Neurology, Donostia University Hospital, San Sebastian, Gipuzkoa, Spain; Neuroscience Area, Biodonostia Health Research Insitute, San Sebastian, Gipuzkoa, Spain
Patricia Alves	Neuroscience Area, Biodonostia Health Research Insitute, San Sebastian, Gipuzkoa, Spain; Department of Educational Psychology and Psychobiology, Faculty of Education, International University of La Rioja, Logroño, Spain
Benjamin Bender	Department of Diagnostic and Interventional Neuroradiology, University of Tübingen, Tübingen, Germany
Carlo Wilke	Department of Neurodegenerative Diseases, Hertie-Institute for Clinical Brain Research and Center of Neurology, University of Tübingen, Tübingen, Germany; Center for Neurodegenerative Diseases (DZNE), Tübingen, Germany
Lisa Graf	Department of Neurodegenerative Diseases, Hertie-Institute for Clinical Brain Research and Center of Neurology, University of Tübingen, Tübingen, Germany
Annick Vogels	Department of Human Genetics, KU Leuven, Leuven, Belgium
Mathieu Vandenbulcke	Geriatric Psychiatry Service, University Hospitals Leuven, Belgium; Neuropsychiatry, Department of Neurosciences, KU Leuven, Leuven, Belgium
Philip Van Damme	Neurology Service, University Hospitals Leuven, Belgium; Laboratory for Neurobiology, VIB-KU Leuven Centre for Brain Research, Leuven, Belgium
Rose Bruffaerts	Department of Biomedical Sciences, University of Antwerp, Antwerp, Belgium; Biomedical Research Institute, Hasselt University, 3500 Hasselt, Belgium
Koen Poesen	Laboratory for Molecular Neurobiomarker Research, KU Leuven, Leuven, Belgium
Pedro Rosa-Neto	Translational Neuroimaging Laboratory, McGill Centre for Studies in Aging, McGill University, Montreal, Québec, Canada
Serge Gauthier	Alzheimer Disease Research Unit, McGill Centre for Studies in Aging, Department of Neurology & Neurosurgery, McGill University, Montreal, Québec, Canada
Agnès Camuzat	Sorbonne Université, Paris Brain Institute – Institut du Cerveau – ICM, Inserm U1127, CNRS UMR 7225, AP-HP - Hôpital Pitié-Salpêtrière, Paris, France
Alexis Brice	Sorbonne Université, Paris Brain Institute – Institut du Cerveau – ICM, Inserm U1127, CNRS UMR 7225, AP-HP - Hôpital Pitié-Salpêtrière, Paris, France; Reference Network for Rare Neurological Diseases (ERN-RND)
Anne Bertrand	Sorbonne Université, Paris Brain Institute – Institut du Cerveau – ICM, Inserm U1127, CNRS UMR 7225, AP-HP - Hôpital Pitié-Salpêtrière, Paris, France; Inria,

	Aramis project-team, F-75013, Paris, France; Centre pour l'Acquisition et le Traitement des Images, Institut du Cerveau et la Moelle, Paris, France
Aurélie Funkiewiez	Centre de référence des démences rares ou précoces, IM2A, Département de Neurologie, AP-HP - Hôpital Pitié-Salpêtrière, Paris, France; Sorbonne Université, Paris Brain Institute – Institut du Cerveau – ICM, Inserm U1127, CNRS UMR 7225, AP-HP - Hôpital Pitié-Salpêtrière, Paris, France
Daisy Rinaldi	Centre de référence des démences rares ou précoces, IM2A, Département de Neurologie, AP-HP - Hôpital Pitié-Salpêtrière, Paris, France; Sorbonne Université, Paris Brain Institute – Institut du Cerveau – ICM, Inserm U1127, CNRS UMR 7225, AP-HP - Hôpital Pitié-Salpêtrière, Paris, France; Département de Neurologie, AP-HP - Hôpital Pitié-Salpêtrière, Paris, France
Dario Saracino	Sorbonne Université, Paris Brain Institute – Institut du Cerveau – ICM, Inserm U1127, CNRS UMR 7225, AP-HP - Hôpital Pitié-Salpêtrière, Paris, France; Inria, Aramis project-team, F-75013, Paris, France; Centre de référence des démences rares ou précoces, IM2A, Département de Neurologie, AP-HP - Hôpital Pitié-Salpêtrière, Paris, France
Olivier Colliot	Sorbonne Université, Paris Brain Institute – Institut du Cerveau – ICM, Inserm U1127, CNRS UMR 7225, AP-HP - Hôpital Pitié-Salpêtrière, Paris, France; Inria, Aramis project-team, F-75013, Paris, France; Centre pour l'Acquisition et le Traitement des Images, Institut du Cerveau et la Moelle, Paris, France
Sabrina Sayah	Sorbonne Université, Paris Brain Institute – Institut du Cerveau – ICM, Inserm U1127, CNRS UMR 7225, AP-HP - Hôpital Pitié-Salpêtrière, Paris, France
Catharina Prix	Neurologische Klinik, Ludwig-Maximilians-Universität München, Munich, Germany
Elisabeth Wlasich	Neurologische Klinik, Ludwig-Maximilians-Universität München, Munich, Germany
Olivia Wagemann	Neurologische Klinik, Ludwig-Maximilians-Universität München, Munich, Germany
Sandra Loosli	Neurologische Klinik, Ludwig-Maximilians-Universität München, Munich, Germany
Sonja Schönecker	Neurologische Klinik, Ludwig-Maximilians-Universität München, Munich, Germany
Tobias Hoegen	Neurologische Klinik, Ludwig-Maximilians-Universität München, Munich, Germany
Jolina Lombardi	Department of Neurology, University of Ulm, Ulm
Sarah Anderl-Straub	Department of Neurology, University of Ulm, Ulm, Germany
Adeline Rollin	CHU, CNR-MAJ, Labex Distalz, LiCEND Lille, France
Gregory Kuchcinski	Univ Lille, France; Inserm 1172, Lille, France; CHU, CNR-MAJ, Labex Distalz, LiCEND Lille, France
Maxime Bertoux	Inserm 1172, Lille, France; CHU, CNR-MAJ, Labex Distalz, LiCEND Lille, France
Thibaud Lebouvier	Univ Lille, France; Inserm 1172, Lille, France; CHU, CNR-MAJ, Labex Distalz, LiCEND Lille, France
Vincent Deramecourt	Univ Lille, France; Inserm 1172, Lille, France; CHU, CNR-MAJ, Labex Distalz, LiCEND Lille, France
Beatriz Santiago	Neurology Department, Centro Hospitalar e Universitario de Coimbra, Coimbra, Portugal

Diana Duro	Faculty of Medicine, University of Coimbra, Coimbra, Portugal
Maria João Leitão	Centre of Neurosciences and Cell Biology, Universidade de Coimbra, Coimbra, Portugal
Maria Rosario Almeida	Faculty of Medicine, University of Coimbra, Coimbra, Portugal
Miguel Tábuas-Pereira	Neurology Department, Centro Hospitalar e Universitario de Coimbra, Coimbra, Portugal
Sónia Afonso	Instituto Ciencias Nucleares Aplicadas a Saude, Universidade de Coimbra, Coimbra, Portugal

GREY MATTER

Cortex

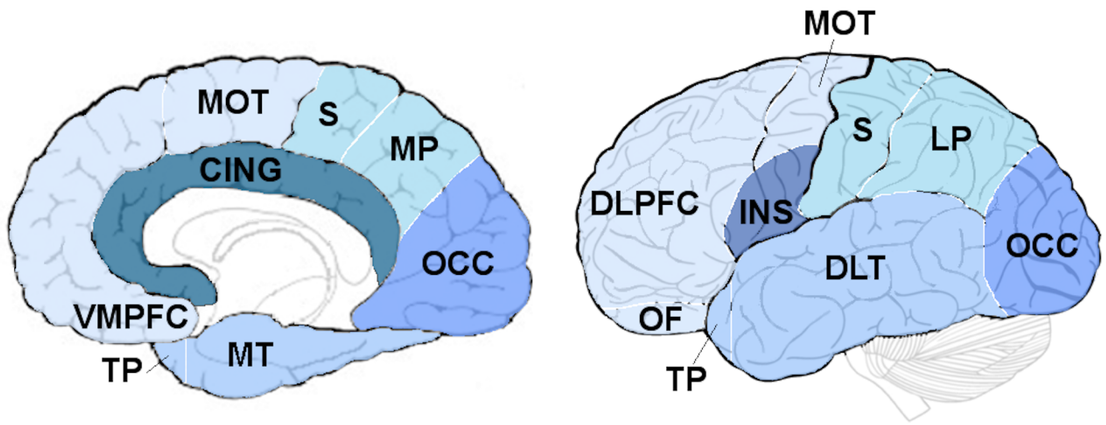

Basal ganglia and Basal forebrain

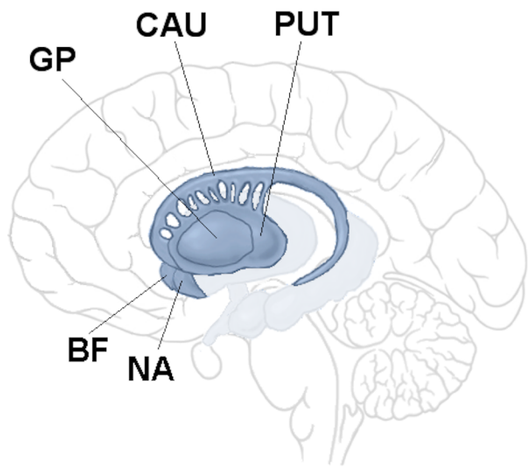

Brainstem and Cerebellum

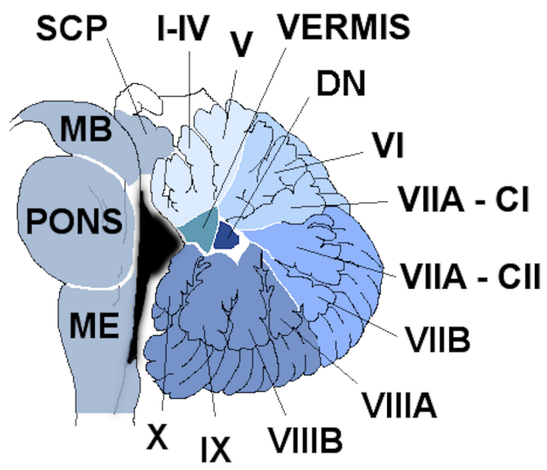

Amygdala

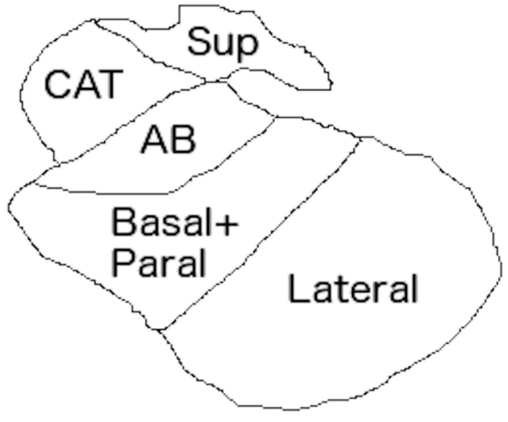

Hippocampus

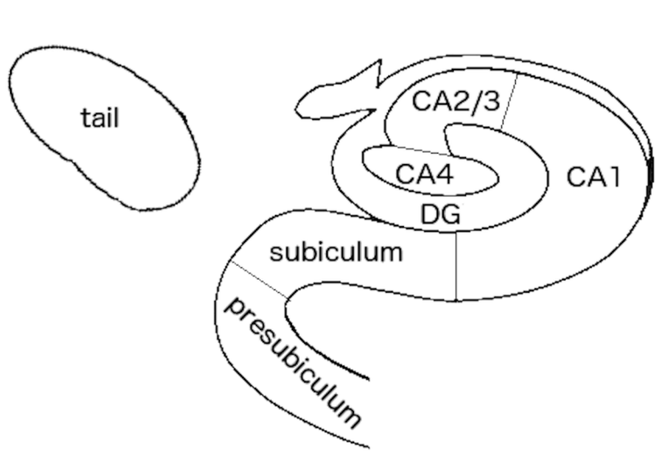

Thalamus

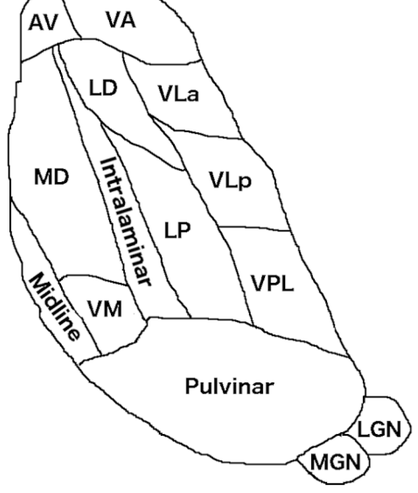

Hypothalamus

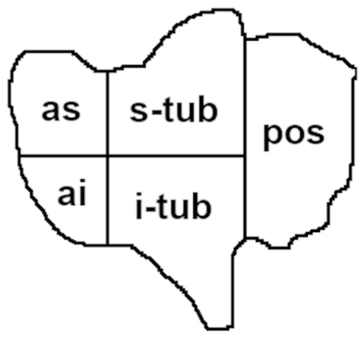

WHITE MATTER

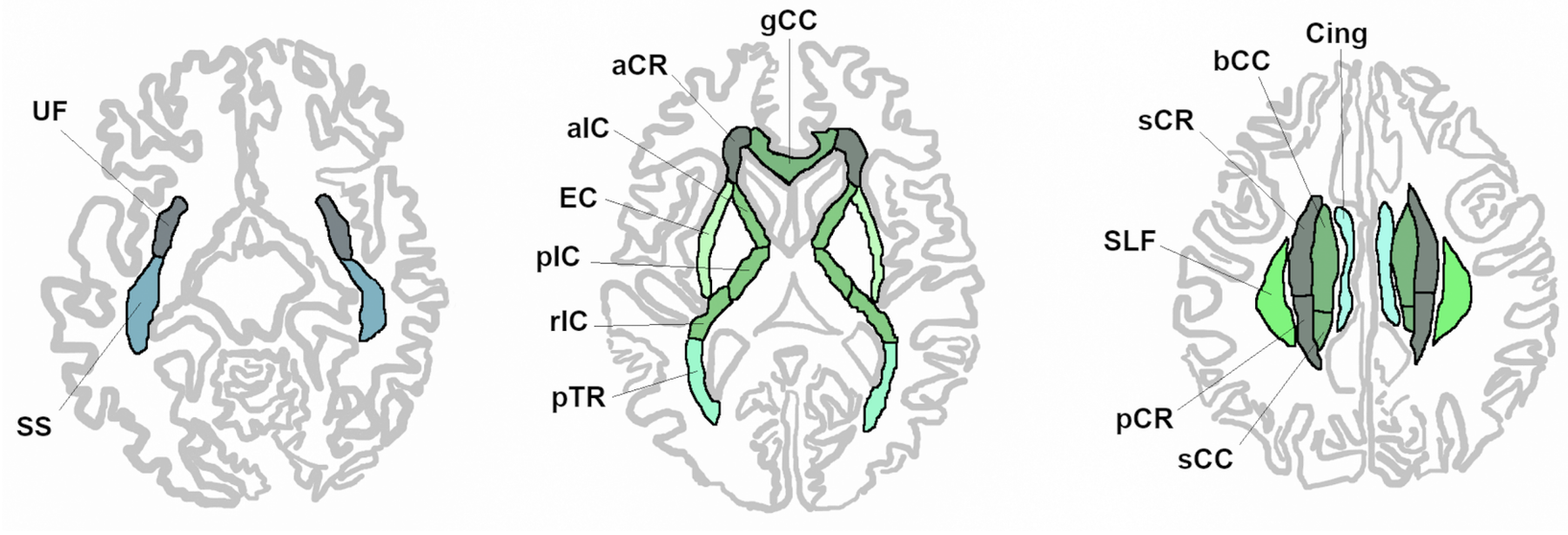

C9orf72

CDR®+NACC FTLD≤0.5

Cortex

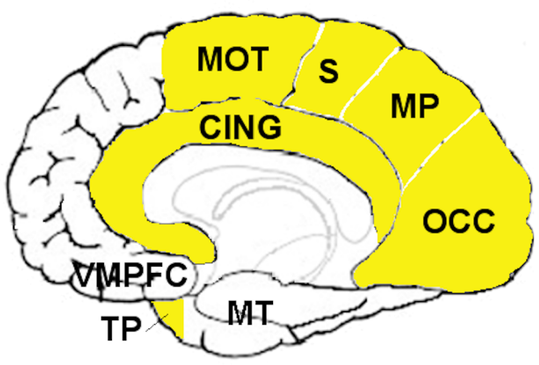

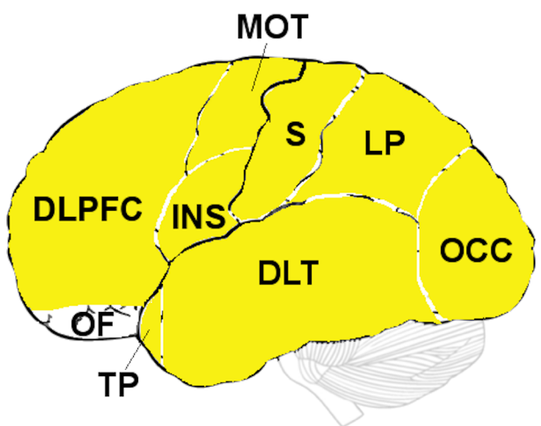

Basal ganglia and Basal forebrain

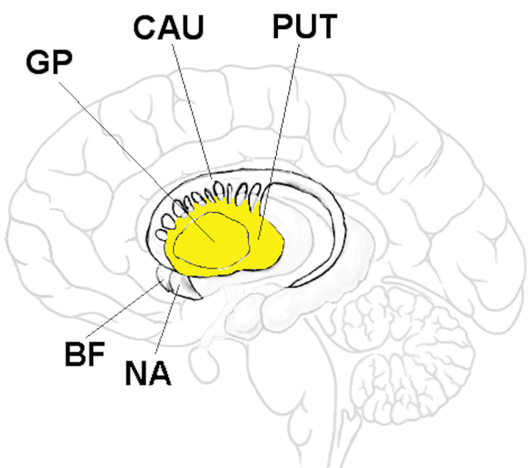

Brainstem and Cerebellum

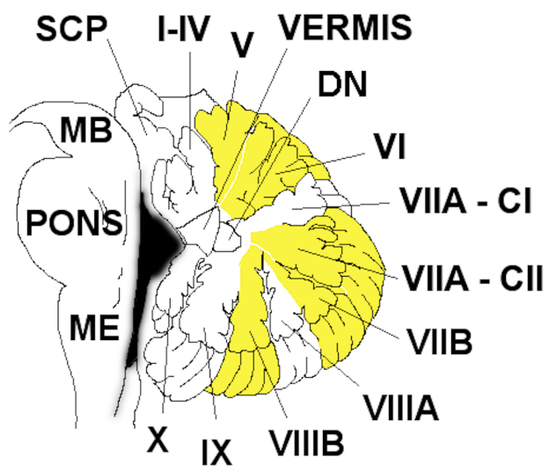

Amygdala

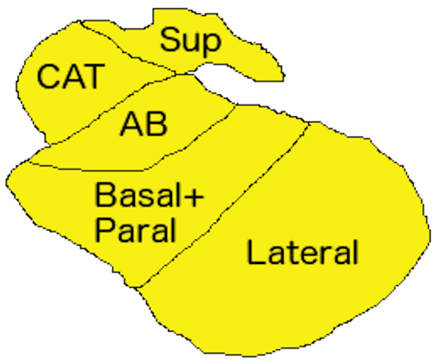

Hippocampus

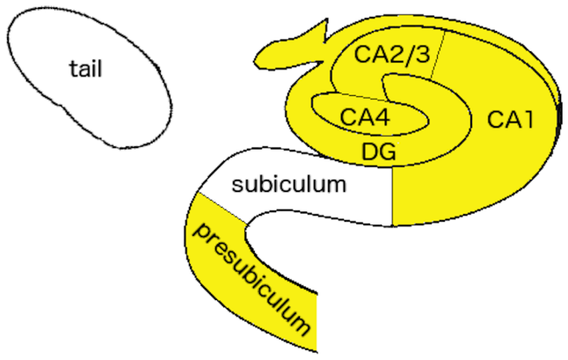

Thalamus

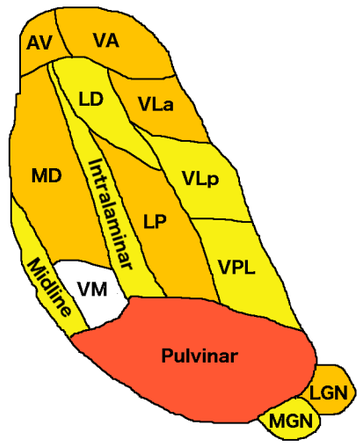

Hypothalamus

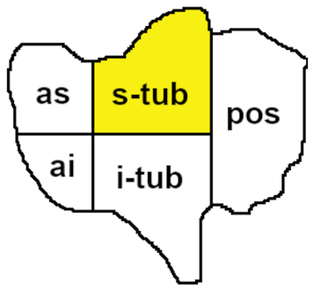

CDR®+NACC FTLD≥1

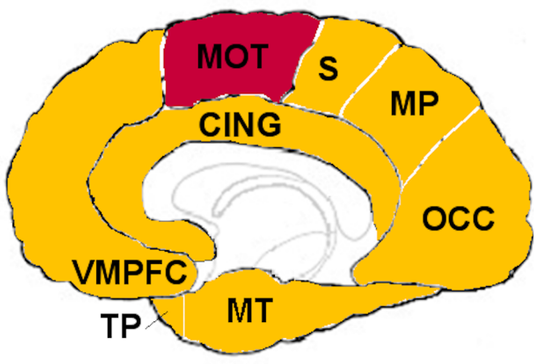

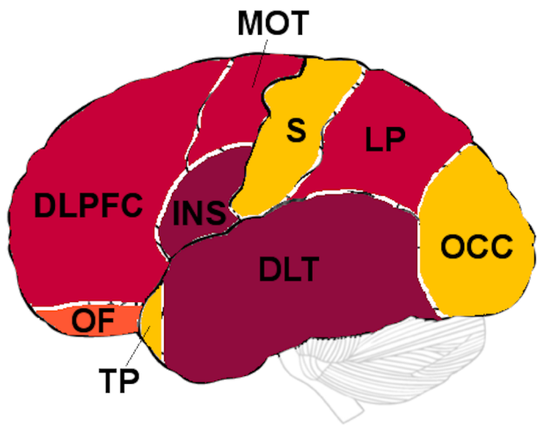

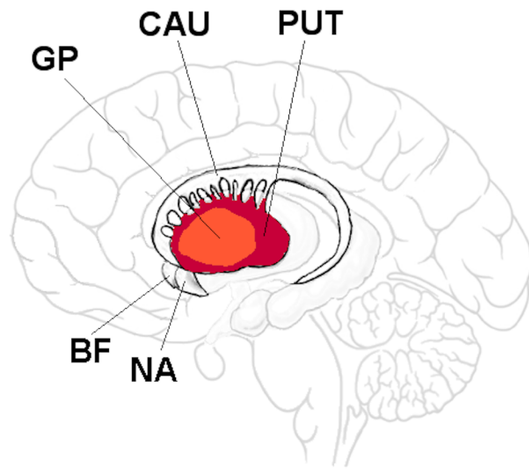

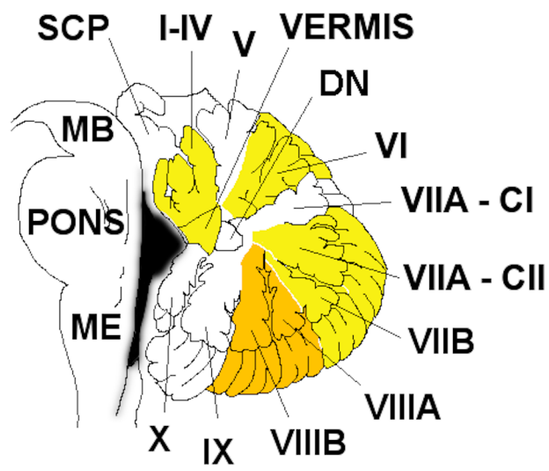

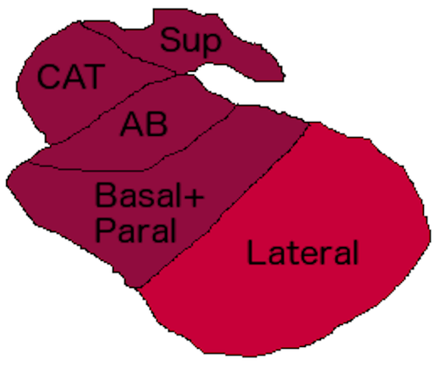

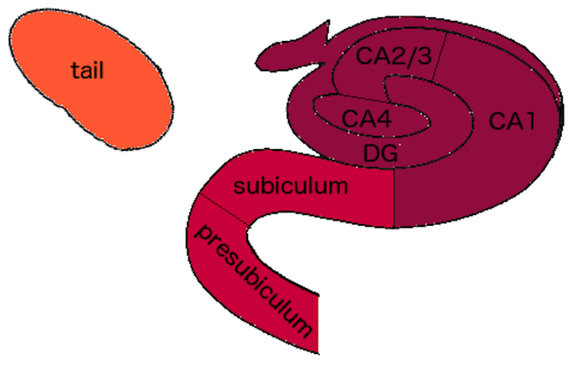

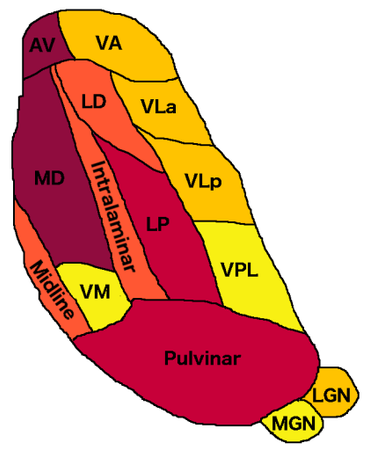

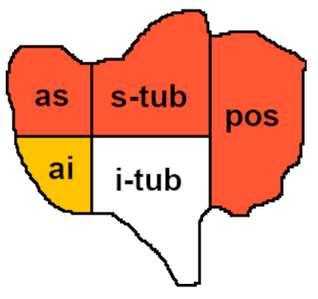

MAPT

CDR®+NACC FTLD≤0.5

Cortex

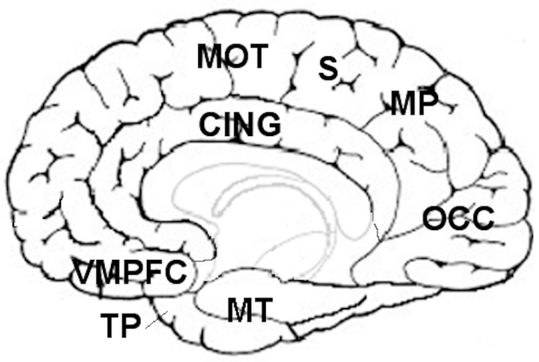

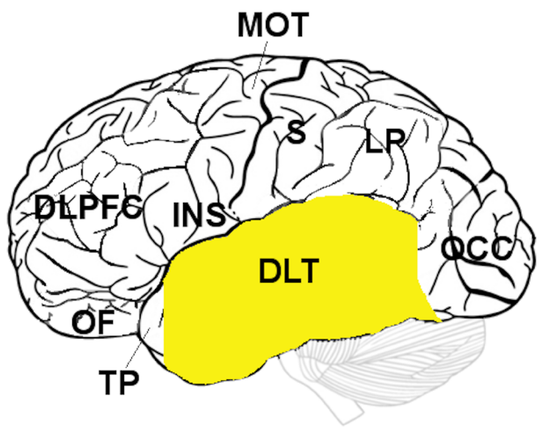

Basal ganglia and Basal forebrain

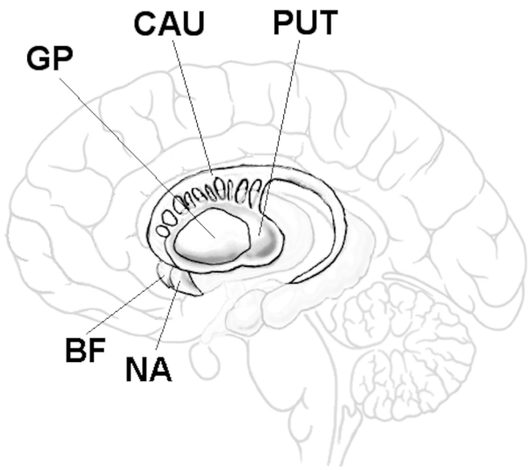

Brainstem and Cerebellum

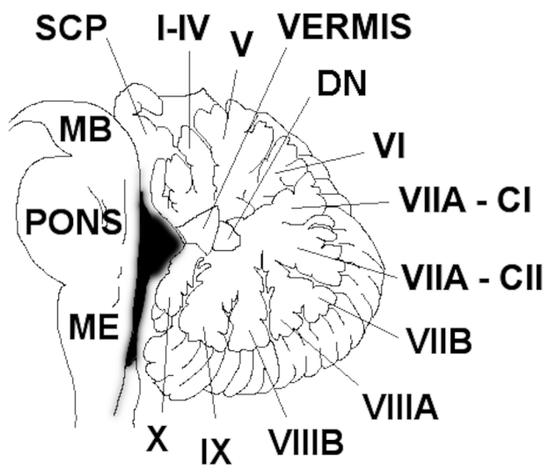

Amygdala

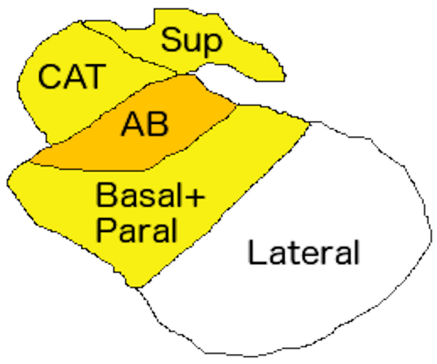

Hippocampus

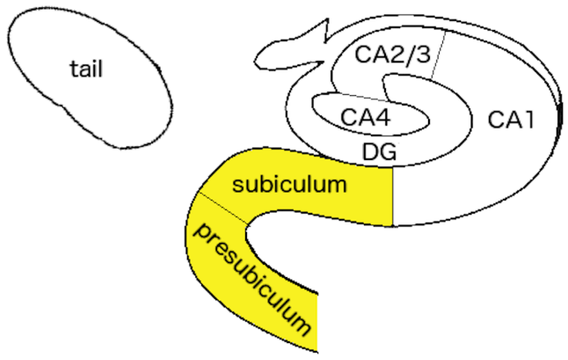

Thalamus

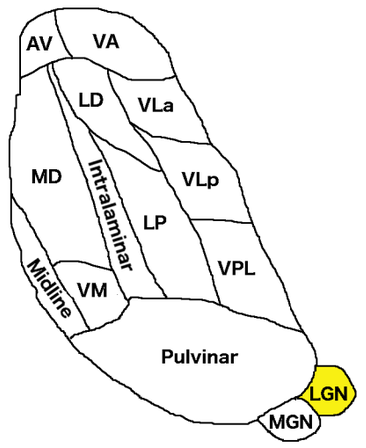

Hypothalamus

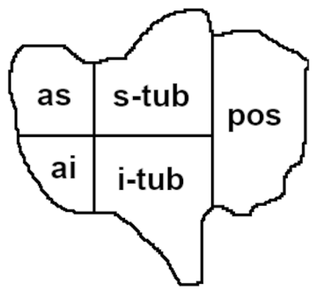

CDR®+NACC FTLD≥1

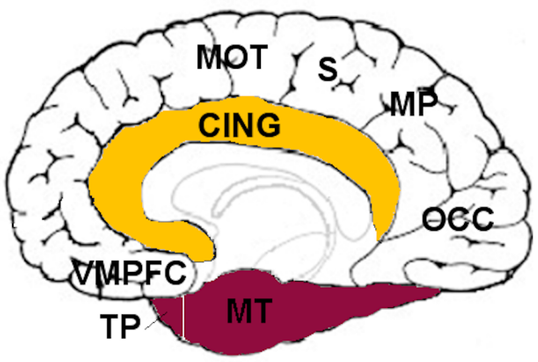

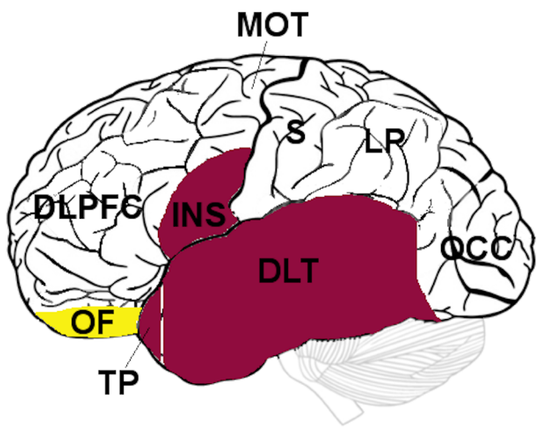

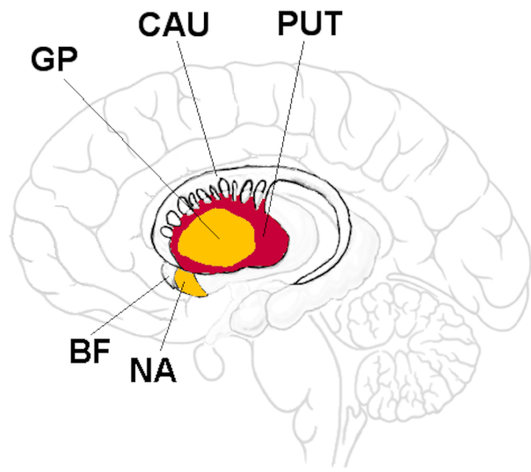

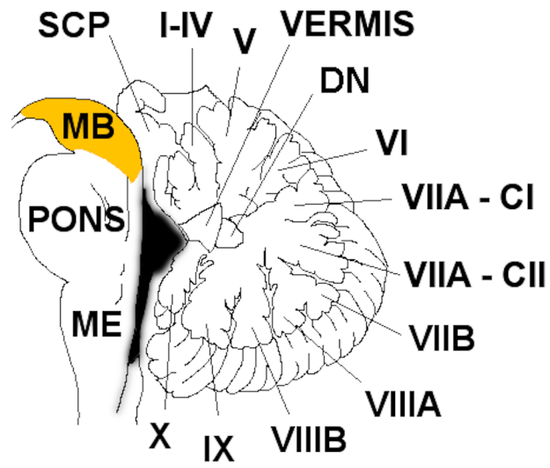

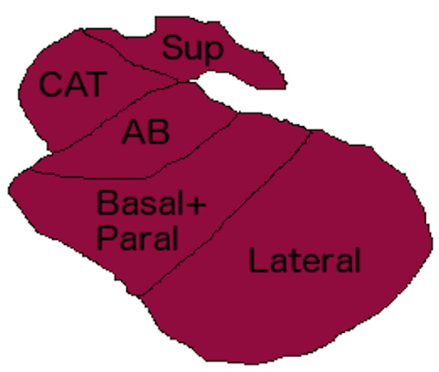

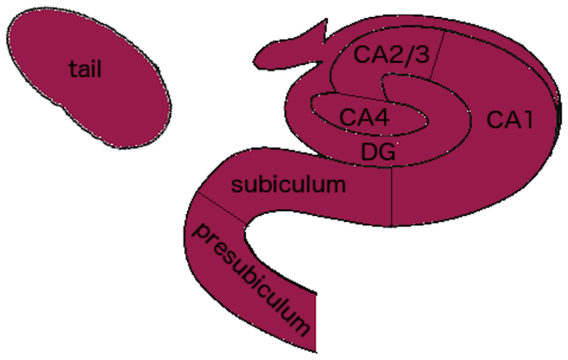

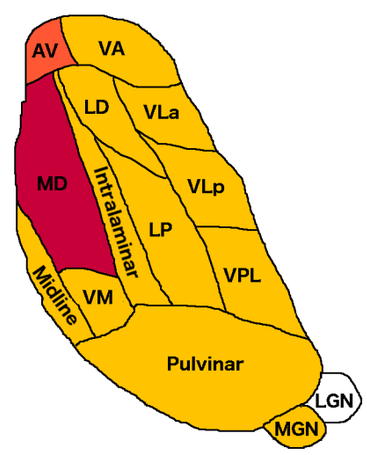

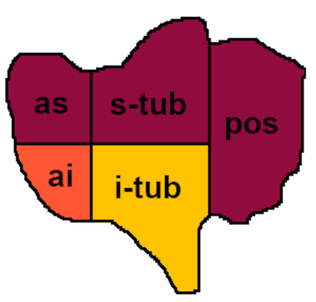

GRN

CDR®+NACC FTLD≤0.5

Cortex

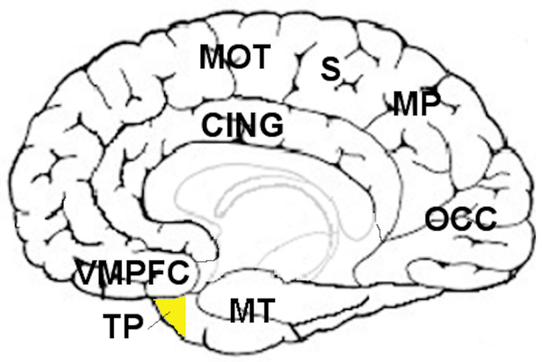

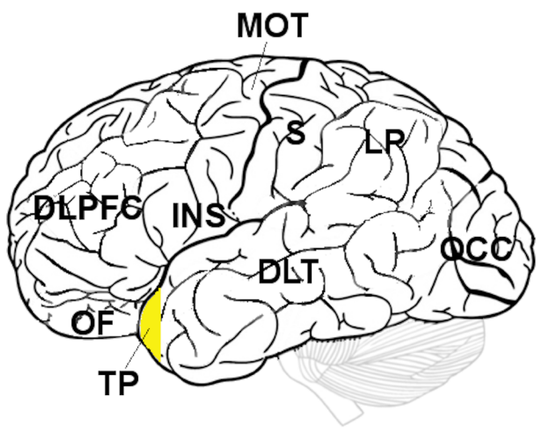

Basal ganglia and Basal forebrain

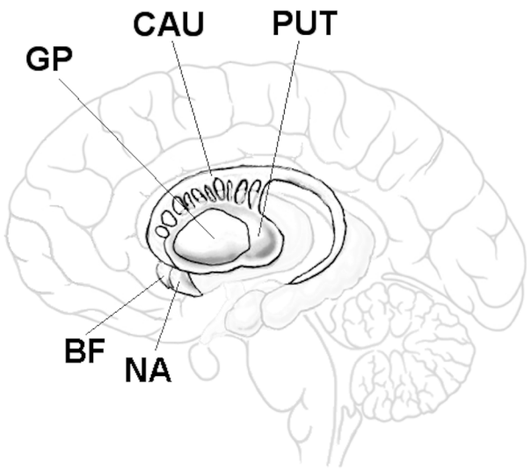

Brainstem and Cerebellum

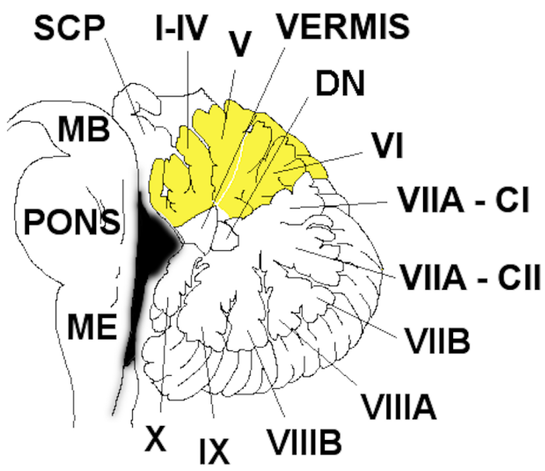

Amygdala

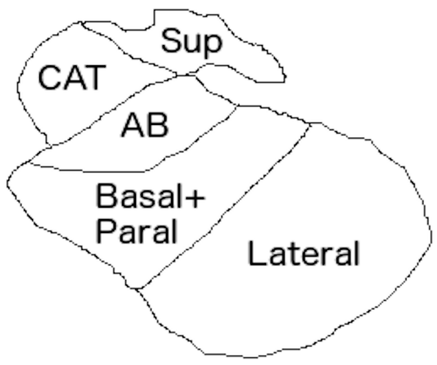

Hippocampus

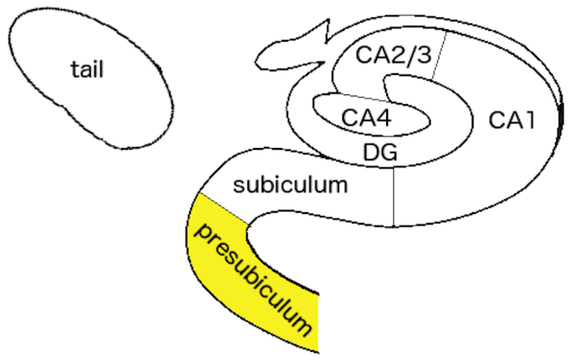

Thalamus

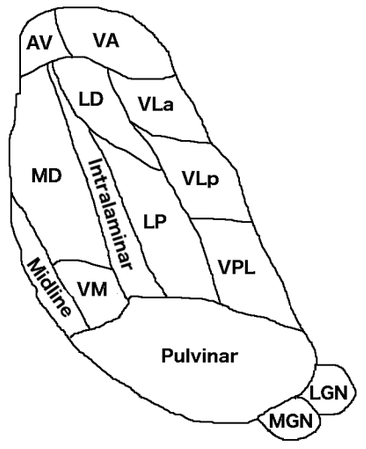

Hypothalamus

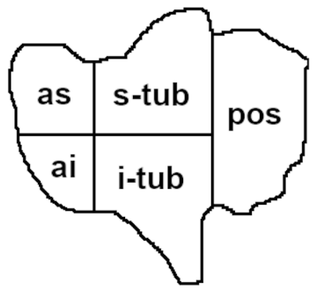

CDR®+NACC FTLD≥1

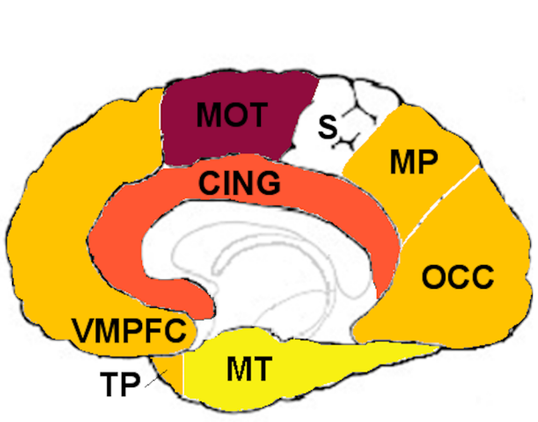

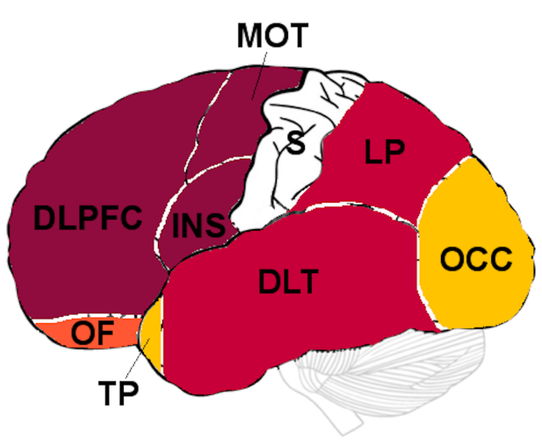

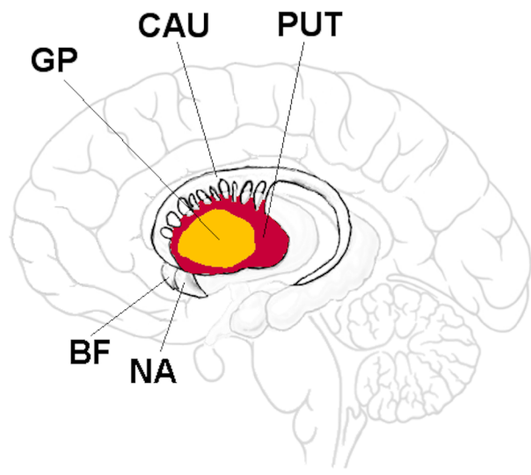

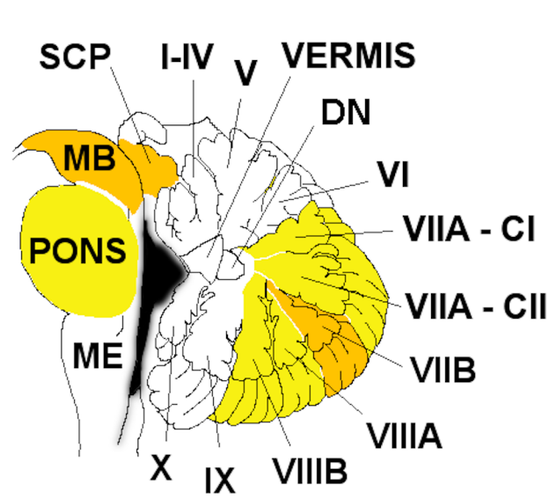

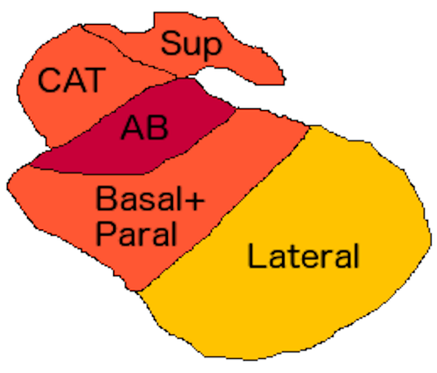

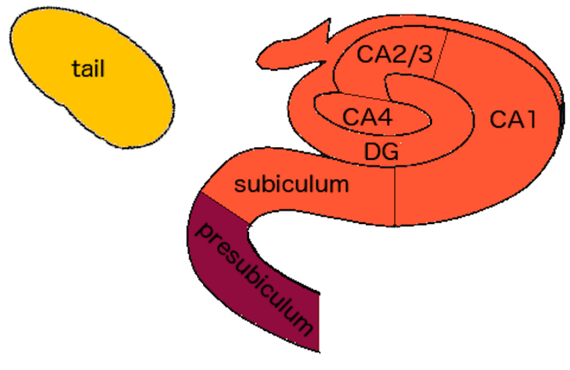

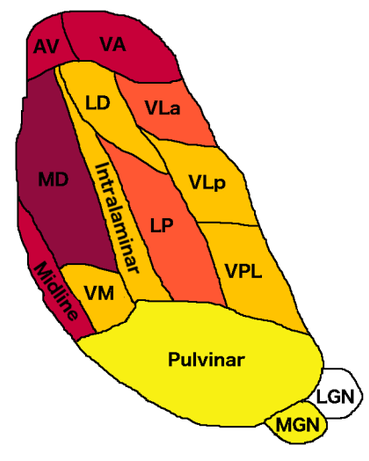

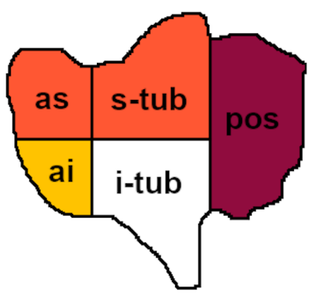

FA

CDR®+NACC FTLD≤0.5

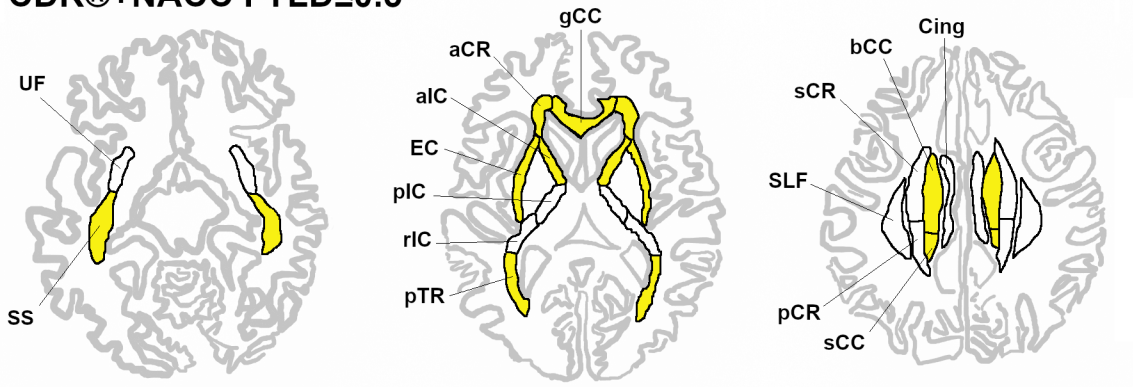

CDR®+NACC FTLD≥1

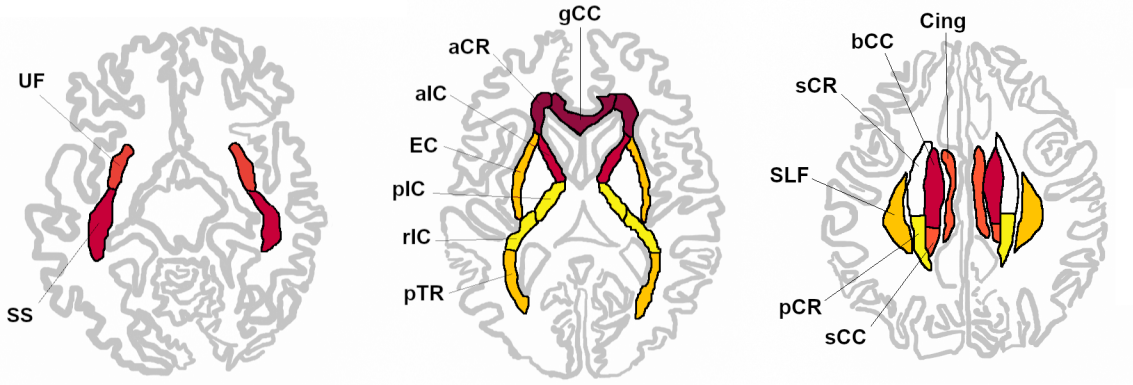

MD

CDR®+NACC FTLD≤0.5

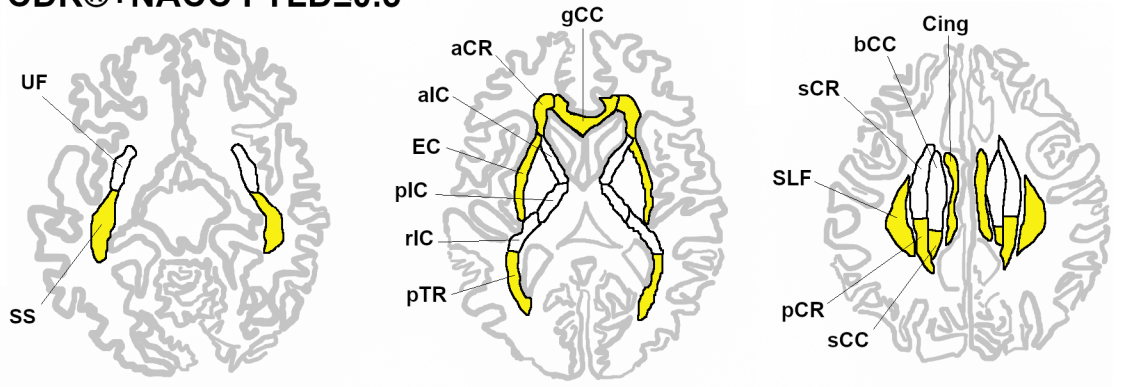

CDR®+NACC FTLD≥1

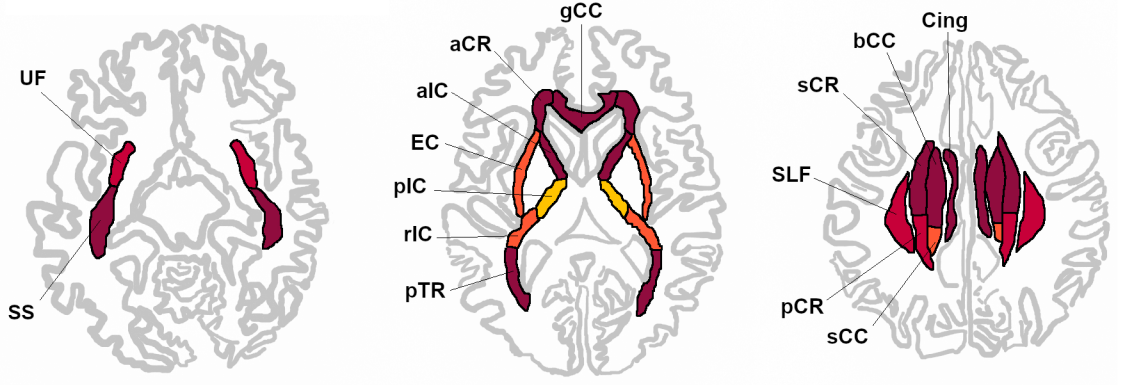

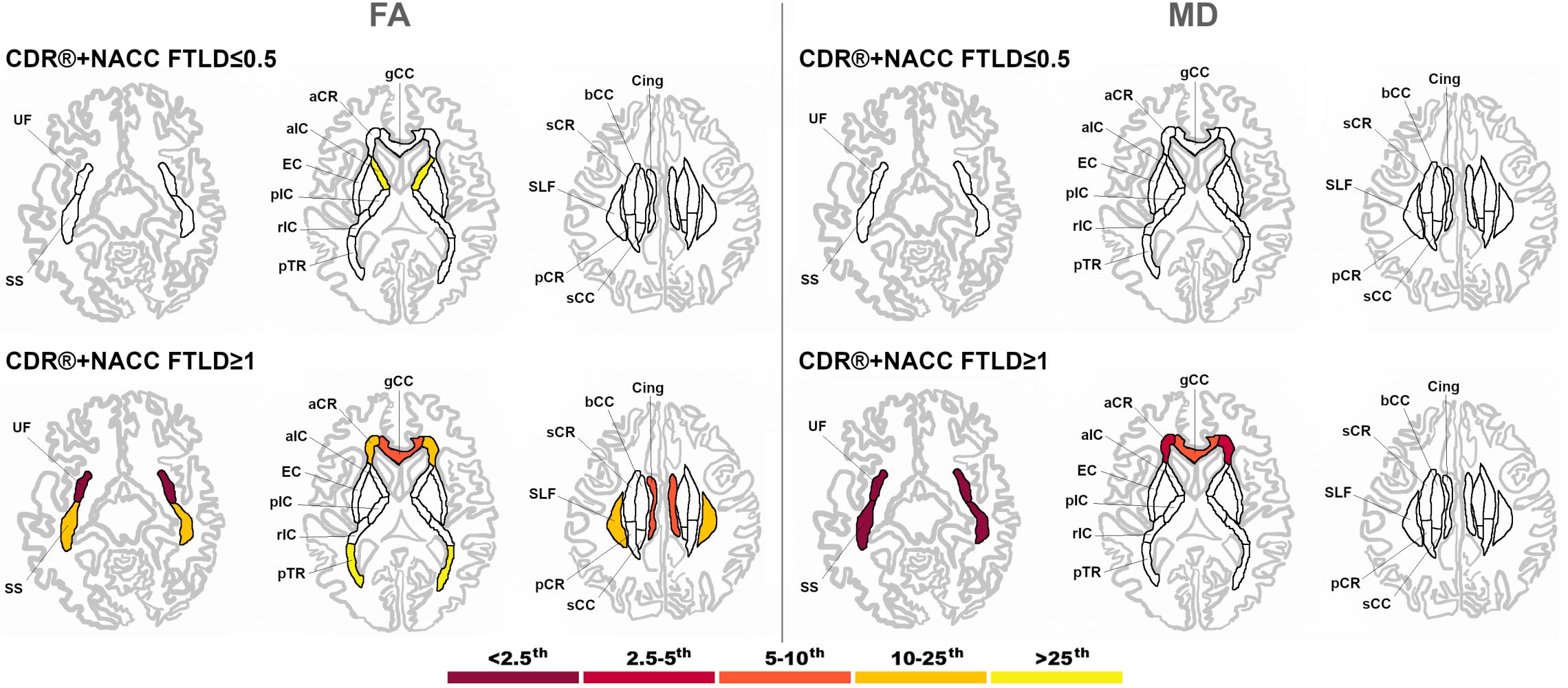
FA
MD
CDR®+NACC FTLD≤0.5
CDR®+NACC FTLD≥1
UF
SS
gCC
aCR
aIC
EC
pIC
rIC
pTR
Cing
bCC
sCR
SLF
pCR
sCC
<2.5th
2.5-5th
5-10th
10-25th
>25th

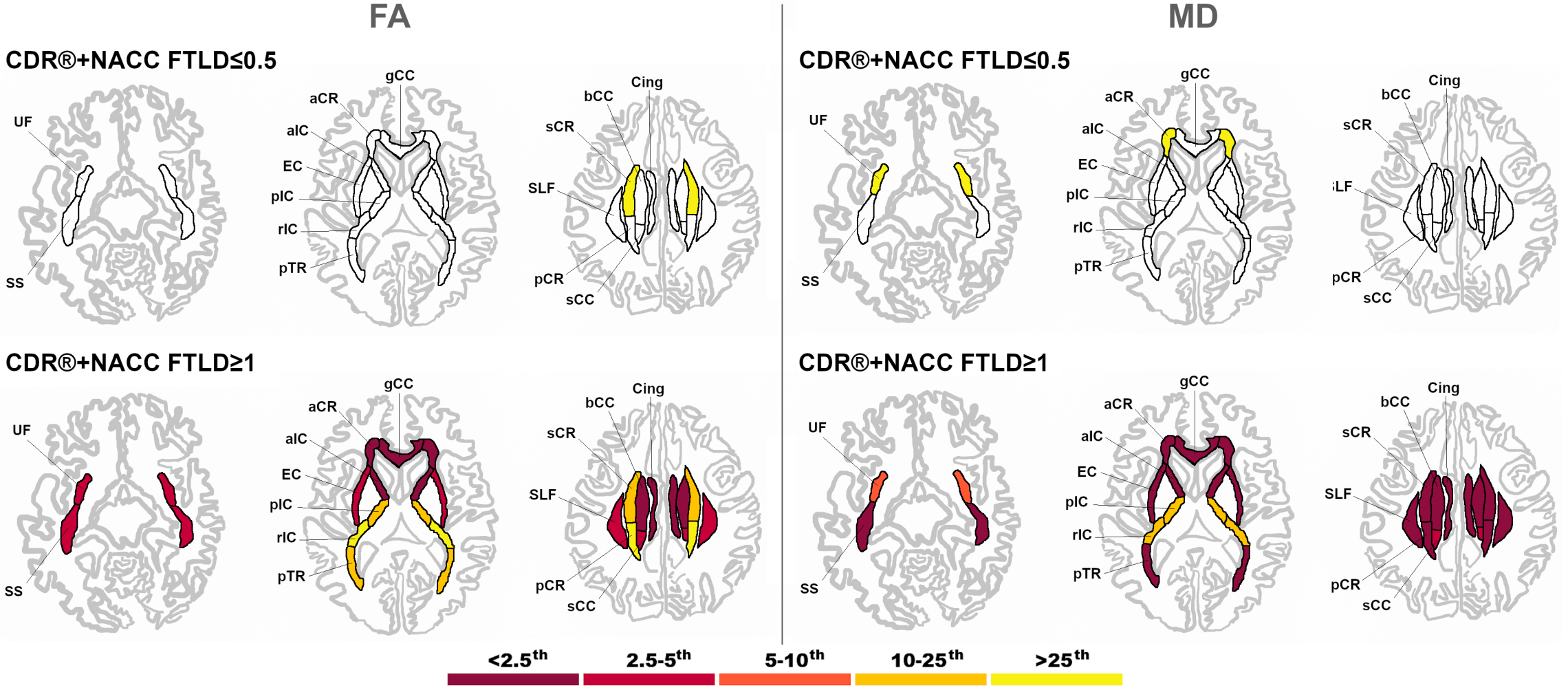
FA
MD
CDR®+NACC FTLD≤0.5
CDR®+NACC FTLD≥1
UF
SS
gCC
aCR
aIC
EC
pIC
rIC
pTR
Cing
bCC
sCR
SLF
pCR
sCC
<2.5th
2.5-5th
5-10th
10-25th
>25th

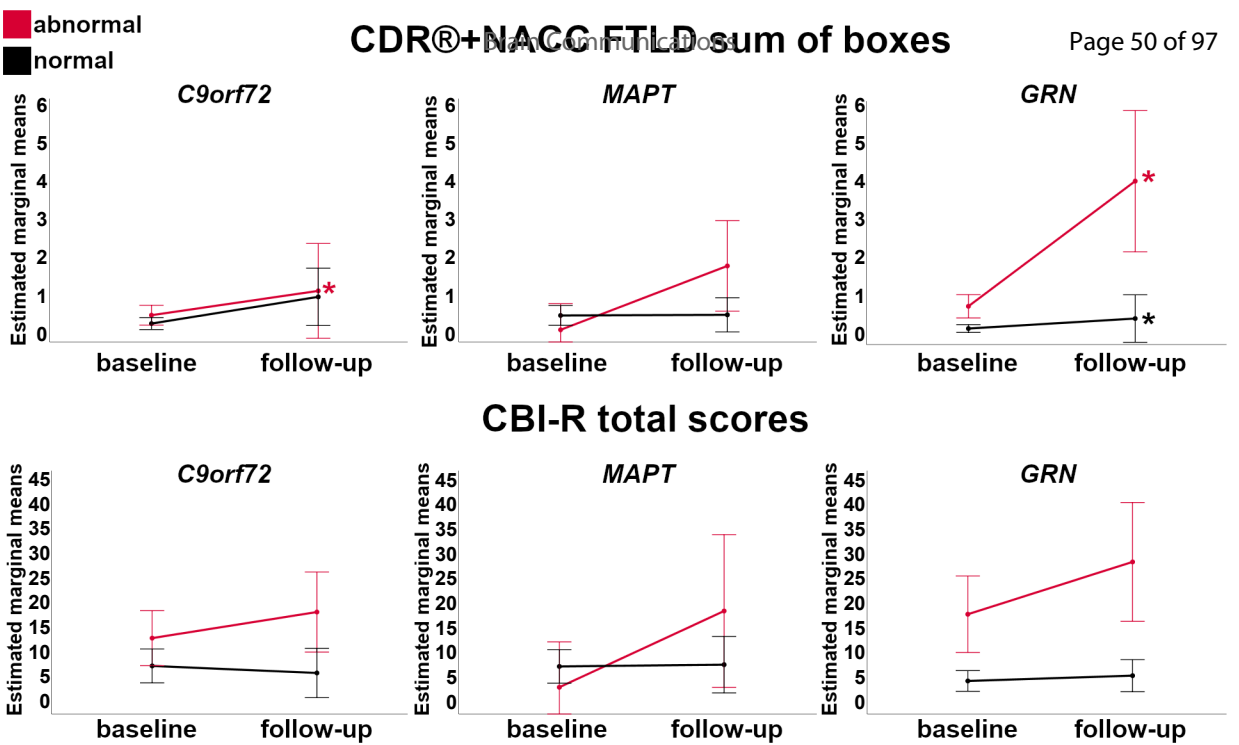
abnormal
normal
CDR®+NACC FTLD sum of boxes
C9orf72
MAPT
GRN
Estimated marginal means
baseline
follow-up
CBI-R total scores
C9orf72
MAPT
GRN
Estimated marginal means
baseline
follow-up

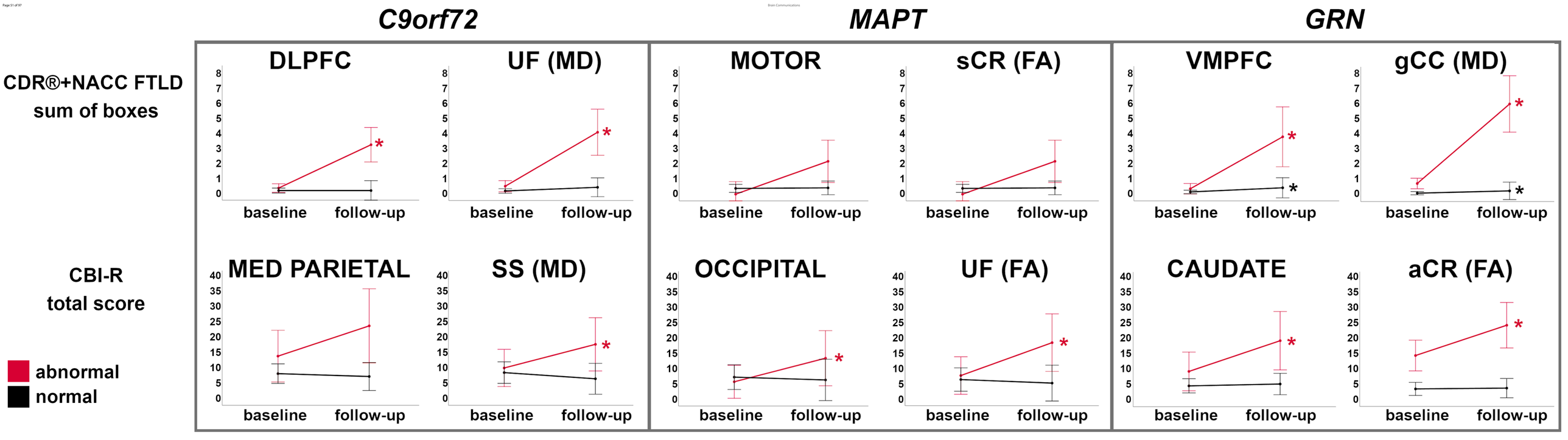
C9orf72
MAPT
GRN
CDR®+NACC FTLD
sum of boxes
CBI-R
total score
abnormal
normal
DLPFC
UF (MD)
MOTOR
sCR (FA)
VMPFC
gCC (MD)
MED PARIETAL
SS (MD)
OCCIPITAL
UF (FA)
CAUDATE
aCR (FA)
baseline
follow-up

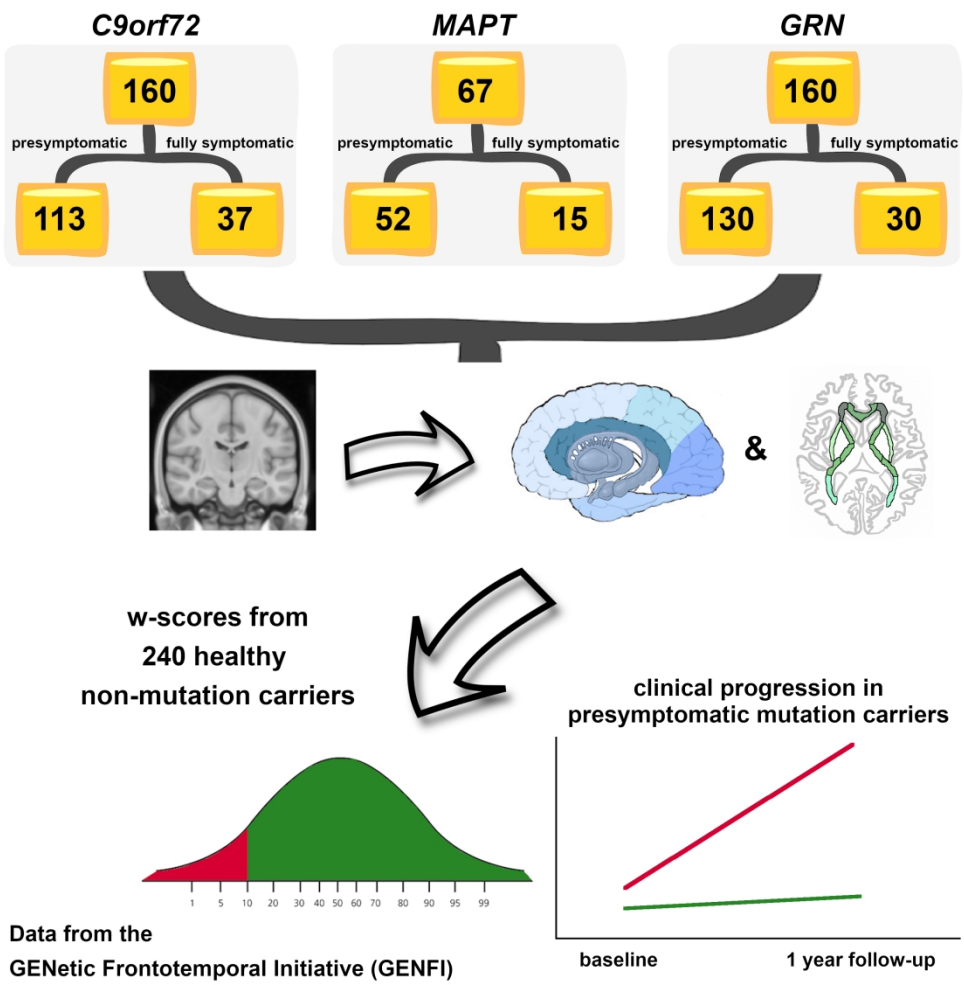

1058x1058mm (72 x 72 DPI)